SIMULATION OF METEOROLOGICAL FIELDS WITHIN AND ABOVE URBAN AND RURAL CANOPIES WITH A MESOSCALE MODEL (MM5) ⋆

SYLVAIN DUPONT⋆⋆, TANYA L. OTTE⋆⋆⋆ and JASON K. S. CHING⋆⋆⋆
NOAA Air Resources Laboratory, Atmospheric Sciences Modeling Division, Research Triangle Park, North Carolina, U.S.A.

(Received in final form 18 November 2003)

Abstract. Accurate simulation of air quality at neighbourhood scales (on order of 1-km horizontal grid spacing) requires detailed meteorological fields inside the roughness sub-layer (RSL). Since the assumptions of the roughness approach, used by most of the mesoscale models, are unsatisfactory at this scale, a detailed urban and rural canopy parameterisation, called DA-SM2-U, is developed inside the Penn State/NCAR Mesoscale Model (MM5) to simulate the meteorological fields within and above the urban and rural canopies. DA-SM2-U uses the drag-force approach to represent the dynamic and turbulent effects of the buildings and vegetation, and a modified version of the soil model SM2-U, called SM2- U(3D), to represent the thermodynamic effects of the canopy elements. The turbulence length scale is also modified inside the canopies. SM2-U(3D) assesses the sensible and latent heat fluxes from rural and urban surfaces in each of the computational layers inside the canopies by considering the shadowing effect, the radiative trapping by the street canyons, and the storage heat flux by the artificial surfaces. DA-SM2-U is tested during one simulated day above the city of Philadelphia, U.S.A. It is shown that DA-SM2-U is capable of simulating the important features observed in the urban and rural RSL, as seen in the vertical profiles of the shear stress, turbulent kinetic energy budget components, eddy diffusivity, potential air temperature, and specific humidity. Within the canopies, DA-SM2-U simulates the decrease of the wind speed inside the dense canopies, the skirting of the flow around the canopy blocks, warmer air inside the vegetation canopy than above open areas during the night and conversely during the day, and constantly warmer air inside the urban canopy. The comparison with measurements shows that the surface air temperature above rural and urban areas is better simulated by DA-SM2-U than by the 'standard version' of MM5.

Keywords: Eddy diffusivity, Energy budget, Mesoscale models, Rural and urban canopies, Urban boundary layer.

⋆ *Disclaimer.* The information in this manuscript has been prepared under funding by the United States Environmental Protection Agency. It has been subjected to Agency review and approved for publication. Mention of trade names or commercial products does not constitute endorsement or recommendation for use.

⋆⋆ Present address: Sylvain Dupont, INRA-EPHYSE, B.P. 81, 33883 Villenauve D'Ornon, France. E-mail: sdupont@bordeaux.inra.fr

⋆⋆⋆ Gn assignment to the National Exposure Research Laboratory, U.S. Environmental Protection Agency.

Boundary-Layer Meteorology **113:** 111–158, 2004.

1. Introduction

As in many atmospheric models, the Penn State/NCAR Mesoscale Model (MM5) (Grell et al., 1994) represents the aerodynamic and thermodynamic characteristics of urban surfaces by applying the roughness approach (RA) and by modifying the parameters of the rural soil model. Thus, the influence of surface obstacles is represented by gridded roughness length and a displacement height, and the surface exchange coefficients are calculated from the Monin–Obukhov similarity theory. It is well known that the RA is unsatisfactory inside the roughness sub-layer (RSL), which is not a constant-flux layer. Additionally, RA requires an implicit assumption of statistical stationarity and spatial homogeneity of the surface roughness elements, which is not verified at neighborhood scales (on order of 1-km horizontal grid spacing) above urban areas. To simulate the urban climatology or the impact of a city on its environment, the RA can be assumed satisfactory if the vertical and horizontal sizes of the first layer cells are large enough, respectively, to include the RSL and to assume an horizontal surface homogeneity. However, since primary atmospheric pollutants are emitted inside the RSL and consequently the first chemical reactions and dispersion occur in this layer, it is necessary to generate detailed meteorological fields inside the RSL to perform air quality modelling at high spatial resolutions. At neighbourhood scale, the meteorological fields are strongly influenced by the presence of the vegetation and building morphology of varying complexity, which requires developing more detailed treatment of the influence of canopy structures in the models and using additional morphological databases as input.

Over the last decade, atmospheric models have been adapted to simulate meteorological fields within and above the vegetation canopy with different turbulent schemes: $E - l$, see Wilson et al. (1998), Zeng and Takahashi (2000); $E - \varepsilon$, Liu et al. (1996); higher-order closure scheme, Meyers and U (1986); large-eddy simulation (LES), Shen and Leclerc (1997), Shaw and Patton (2003), Kanda and Hino (1994); and transilient turbulent theory, see Inclan et al. (1996), Ni (1997). All of these models represent the vegetation dynamic effects by adding a pressure and viscous drag force in the momentum equation, called hereafter the drag-force approach (DA), and, following the turbulent scheme, by adding a source and/or sink term in the turbulent kinetic energy (TKE) and in the dissipation rate equations, and by modifying the turbulent length scale (TLS) parameterisation inside the canopy. With the DA, the lowest level of the computational domain corresponds to the real level of the ground, and additional vertical layers are included within the vegetation canopy to allow more detailed meteorological fields in the RSL.

Recently, the DA has been extended to the building canopy by Brown (2000), Ca et al. (2002), Martilli et al. (2002) and Lacser and Otte (2002) for $E - l$ and $E - \varepsilon$ turbulent schemes. Most of these schemes have only been developed for a building canopy without vegetation, or by using a DA for the building representation and a RA for the vegetation. However, the use of the latter method can

be controversial when the lowest model layer is thin, because the assumptions of the Monin-Obukhov similarity theory used by the RA cannot be applied near the ground since the constant flux layer is nonexistent.

This paper presents a new version of MM5, called hereafter DA-SM2-U, which is able to simulate all meteorological fields within and above the rural and urban canopies. This new version uses the DA to represent the dynamic and turbulent effects, (i) of the buildings following the work of Lacser and Otte (2002) and Martilli et al. (2002), and (ii) of the vegetation. The DA is developed inside the $E - l$ Gayno-Seaman planetary boundary layer (GSPBL) model (Shafran et al., 2000).

The simulation of the meteorological fields within the rural and urban canopies needs also to consider the heat fluxes from the different in-canopy elements. The assessment of these heat fluxes is complex because of the heterogeneity of the canopies and the different physical processes occurring inside the canopy, e.g., shadowing effects, radiative trapping inside the street canyon, heat storage, vegetation transpiration, evaporation from the bare soil and from the water intercepted by the canopy element. These physical processes influence the flow inside the canopies as well as throughout the planetary boundary layer (PBL), e.g., the urban heat island development. They also influence the pollutant exchanges between the canopies and the atmosphere above. Thus, to have a detailed representation of the complex thermodynamic processes, the DA is coupled with a modified version of the soil model SM2-U (Dupont et al., 2002), called SM2-U(3D), which is capable of determining the heat fluxes and surface temperatures in each in-canopy computational cell following the vertical distribution of the vegetation and buildings.

DA-SM2-U is tested during one simulated day on a real case above the city of Philadelphia, in Pennsylvania, U.S.A. We provide a limited evaluation of DA-SM2-U because of the lack of three-dimensional observations and because of the use of simplified urban and vegetation canopy morphology databases. However, the DA-SM2-U behaviour within the RSL is analysed in depth through the turbulent, air temperature, air specific humidity, and eddy diffusivity fields and through the heat fluxes from the canopy elements. The results here are compared with previous simulations and with observations found in the literature. We also try to explain the implications of these results on the simulation of pollutant concentration in urban areas.

Section 2 describes the variables representing the morphological characteristics of the canopy elements considered by DA-SM2-U. The modifications introduced inside the MM5 meteorological equations to use the DA are presented in Section 3, while Appendix A describes the parameterisation of the vertical turbulent transport and of the eddy diffusivity. Section 4 describes the new soil model SM2-U(3D) adapted for the DA, while the surface temperature and heat flux equations are given in Appendix B.

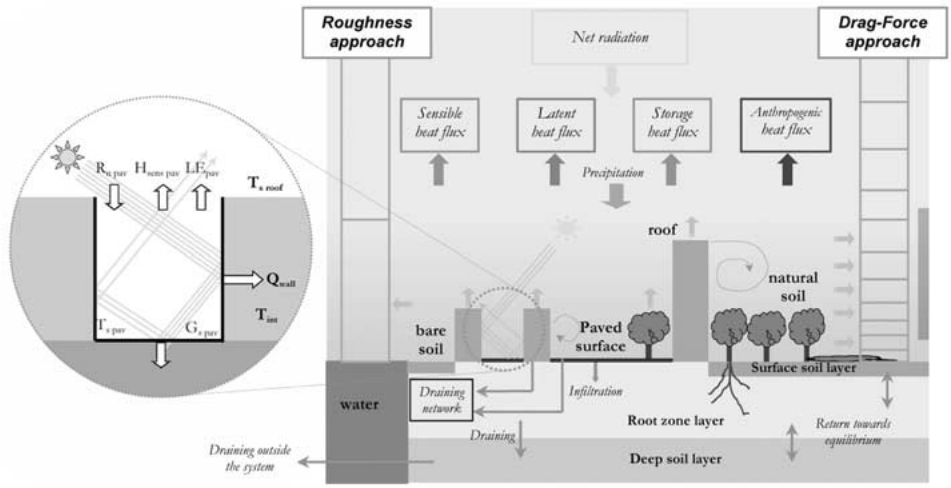

Figure 1. Scheme of the new MM5 canopy parameterisation, DA-SM2-U, using the drag-force approach with the soil model SM2-U, compared with the RA-SM2-U version using the roughness approach.

The model set-up on Philadelphia is presented in Section 5. In Section 6, the vertical profiles of several key variables are analysed and compared with the profiles from the standard version of MM5 and from a MM5 version coupling the RA with SM2-U. In Section 7, the DA-SM2-U surface air temperature and wind speed are compared with observations from several urban and rural stations, and the surface heat fluxes simulated by SM2-U(3D), and their vertical distribution inside the canopy are studied. Finally, the meteorological fields within and just above the canopy are analysed in Section 8.

2. Urban Canopy Representation

As represented in Figure 1, DA-SM2-U considers eight surface types: bare soil located between the sparse vegetation elements, denoted 'nat'; bare soil without vegetation, 'bare'; vegetation over the bare soil, 'vegn'; vegetation over paved surfaces, 'vega', which represents, e.g., trees on road side; paved surfaces located between the sparse vegetation elements, 'pav'; paved surface located under the vegetation, 'cova' (this surface is only used for the water budget); building roofs, 'bui'; and water surfaces, 'wat'. In the equations, the surface types are characterized by the index j.

Unlike the RA, there are some vertical layers inside the canopy with the DA (see Figure 1). Each of the eight surface types is characterized in a cell by its top area density, $\mathrm{Surf}_j(k)$ ($\mathrm{m}^2\ \mathrm{m}^{-2}$), at the level k above the ground (i.e., the ratio between the top area of the surface type 'j' at the level k and the entire top area of

the surface 'j' projected vertically at the ground level), where $k = 0$ corresponds to the ground level and $k = k_{\text{top}}$ to the upper layer of the canopy. Hence, for each surface type:

$$\sum_{k=0}^{k_{\text{top}}} \text{Surf}_j(k) = 1. \tag{1}$$

$\text{Surf}_j(k = 0)$ is equal to zero for roofs (no roof at the ground level), and $\text{Surf}_j(k > 0)$ is equal to zero for bare soils, paved surfaces (overpasses are not considered) and water surfaces. These top area densities are considered as heat exchange surface densities where heat fluxes are emitted. Hence, for simplification, the vegetation exchange surfaces correspond to the upper horizontal surfaces of the vegetation.

The horizontal surface density of the surface type 'j' is denoted f_j ($\text{m}^2\ \text{m}^{-2}$) (i.e., the ratio between the top area of the surface type 'j' projected vertically at the ground level and the area of the horizontal section of the computational cell). Hence,

$$\sum_j f_j = 1 \tag{2}$$

for $j \in \{\text{bare, bui, nat, pav, vega, vegn, wat}\}$.

The total top area density at the level k is defined by

$$\text{Surf}_{\text{tot}}(k) = \sum_j f_j \, \text{Surf}_j(k). \tag{3}$$

The frontal area density ($\text{m}^2\ \text{m}^{-3}$) and plan area density ($\text{m}^2\ \text{m}^{-3}$) of the surface type '$j$' at the level k are $A_{fj}(k)$ and $A_{pj}(k)$, respectively. The first parameter indicates the wind obstacles represented by the element 'j', and the second parameter represents the area at the level k occupied by the element 'j' in the canopy.

We assume the volume of the vegetation in a computational cell to be negligible (Kanda and Hino, 1994) but not the building volume. Thus, we define the horizontal air density, $S_{\text{air}}(k)$, at the level k (i.e., the ratio between the air area at the level k and the area of the horizontal section of the computational cell) by

$$S_{\text{air}}(k) = (1 - f_{\text{bui}}) + \sum_{p=0}^{k-1} f_{\text{bui}} \text{Surf}_{\text{bui}}(p), \tag{4}$$

where the first term on the right-hand side of Equation (4) corresponds to the air area at the ground level, and the second term is the roof area from the ground to the level $k - 1$ that corresponds to the additional air area at the level k to the ground air area. The volume air density ($\text{m}^3\ \text{m}^{-2}$), $V_{\text{air}}(k)$, at the level k is defined by

$$V_{\text{air}}(k) = \int_{z(k)-0.5\Delta z(k)}^{z(k)+0.5\Delta z(k)} S_{\text{air}}(z')dz', \tag{5}$$

where z is the altitude above the ground and Δz is the vertical thickness of the cell.

3. Description of Modifications of the MM5 Meteorological Model

To consider the effect of buildings and vegetation on the flow inside the canopy, the MM5 conservation equations have been modified. These modifications have been implemented inside the GSPBL scheme, which is a $E - l$ turbulence closure model, i.e., the eddy diffusivity is evaluated from the mean TKE and the turbulent length scale.

Note that the parameterisation of the vertical turbulent transport terms has been modified to consider the building volume (see Appendix A).

3.1. Momentum equation

Inside the canopy, the momentum flux is absorbed by the vegetation and buildings by the pressure and viscosity forces. Thus, the momentum equations are

$$\frac{\partial \rho \langle u_i \rangle}{\partial t} = R_{ui} + F_{ui}^{\text{bui}} + \sum_j D_{ui}^j, \tag{6}$$

where $j \in \{\text{bui,vega, vegn}\}$, $i \in \{x, y\}$, $\langle\ \rangle$ denotes the Reynolds averaged variables, u_i is the horizontal wind speed component, ρ is the air density, and R_{ui} represents the general forcing terms in the equation of $\langle u_i \rangle$.

The second term on the right-hand side of Equation (6), F_{ui}^{bui}, corresponds to momentum sources due to the presence of horizontal surfaces of buildings. At the level k inside the canopy, this term is deduced in the same way as the friction force induced by the ground:

$$F_{ui}^{\text{bui}}(k) = -\left(\frac{\rho(k)}{V_{\text{air}}(k)}\right) \frac{f_{\text{bui}} \text{Surf}_{\text{bui}}(k) [u_{*\text{bui}}(k)]^2 \langle u_i(k) \rangle}{(\langle u_x(k) \rangle^2 + \langle u_y(k) \rangle^2)^{0.5}}, \tag{7}$$

where $u_{*\text{bui}}$ is the friction velocity induced by roofs.

The value for $u_{*\text{bui}}$ is assessed from the non-iterative method of Guilloteau (1998) based on the Monin–Obukhov similarity theory taking into account the atmospheric stratification through the roof surface temperature, and the aerodynamic and thermal roughness lengths of roofs. For simplicity, we use this parameterisation to determine $u_{*\text{bui}}$, although the assumptions may not be generally appropriate at this scale.

The third term on the right-hand side of Equation (6) corresponds to momentum sources due to the pressure and viscous drag force induced by the presence of the vegetation and of the building vertical surfaces. It is parameterised as:

$$D_{ui}^j(k) = -\rho(k) C_{dj} A_{fj}(k) \langle u_i(k) \rangle \sqrt{\langle u_x(k) \rangle^2 + \langle u_y(k) \rangle^2}, \tag{8}$$

where $j \in \{\text{bui, vega, vegn}\}$, and C_{dj} is the effective drag coefficient of the element 'j'.

This parameterisation of the drag force term has been initially proposed for the vegetation canopy (c.f. Kaimal and Finnigan, 1994; Raupach et al., 1986; Finnigan, 2000). It has been extended to the building canopy by Raupach et al. (1991), Martilli et al. (2002), Ca et al. (2002) and Lacser and Otte (2002).

The effective drag coefficient of a building canopy or a vegetation canopy is respectively smaller than the drag coefficient of one building or one leaf because of shelter effects. For simplification, the drag forces induced by buildings and vegetation are separated in our model, thus the shelter effects between buildings and vegetation are neglected, which is certainly a large assumption. Some values of C_{dveg} can be found for different types of vegetation canopy in Zeng and Takahashi (2000) and Meyers and U (1986). In our study, we assume that the drag coefficient is vertically constant and we have chosen $C_{\text{dbui}} = 0.4$, as used by Martilli et al. (2002), and $C_{\text{dvegn}} = C_{\text{dvega}} = 0.2$.

3.2. THERMAL EQUATION

The sensible heat fluxes from roofs and vegetation, as well as the anthropogenic heat flux, are added to the liquid-water potential air temperature equation:

$$\frac{\partial \rho \langle \theta_L \rangle}{\partial t} = R_\theta + D_\theta + A_\theta, \tag{9}$$

where θ_L is the liquid-water potential temperature ($\theta_L = \theta - Lq_L/(c_p\pi)$ where θ is the potential temperature, L is the latent heat of evaporation, π is the Exner pressure function, q_L the cloud-water mixing ratio, and c_p the specific heat of air), and R_θ represents the general forcing terms in the equation of $\langle \theta_L \rangle$.

The second term on the right-hand side of Equation (9), D_θ, corresponds to the sensible heat sources from roofs and the vegetation:

$$D_\theta(k) = \left(\frac{1}{V_{\text{air}}(k)}\right) \frac{H_{\text{sens mean}}(k)}{c_p}, \tag{10}$$

where $H_{\text{sens mean}}(k)$ is the sensible heat flux emitted at the level k by buildings and vegetation per unit of ground (see Equation (23) for details).

The third term on the right-hand side of Equation (9), A_θ, corresponds to the heat source from anthropogenic heat flux Q_{urb} emitted, for example, by vehicles and residential heating/cooling (see Equation (B9) for details):

$$A_\theta(k) = \left(\frac{1}{V_{\text{air}}(k)}\right) \frac{Q_{\text{urb}}(k)}{c_p}. \tag{11}$$

3.3. HUMIDITY EQUATION

The humidity sources within the canopy (except from the ground) are the evapotranspiration from the vegetation and the evaporation of the water intercepted by buildings. They are added in the total air water content equation:

$$\frac{\partial \rho \langle q_w \rangle}{\partial t} = R_q + D_q, \tag{12}$$

where q_w is the total water content equal to the sum of the specific humidity and the liquid water content, and R_q represents the general forcing terms in the equation of $\langle q_w \rangle$.

The second term on the right-hand side of Equation (12), D_q, corresponds to the humidity sources from buildings and vegetation:

$$D_q(k) = \frac{E_{\text{mean}}(k)}{V_{\text{air}}(k)}, \tag{13}$$

where E_{mean} is the humidity flux per unit of ground from surfaces located at the level k inside the canopy (see Equation (23) for details).

3.4. TURBULENT KINETIC ENERGY EQUATION

The adaptation of the TKE equation within the canopy to include the building and vegetation effects is delicate because of the complex energy transformations occurring at different spatial and time scales. Within the vegetation canopy, the shear and buoyancy productions of TKE induce larger eddies than the wake production, and the TKE dissipation occurs through the smallest eddies (at the Kolmogorov scale). To consider this difference of scale processes, Wilson (1988) split TKE into two frequency bands by solving a shear kinetic energy equation and a wake kinetic energy equation. Here, so as not to increase the computational time of the model, our TKE represents the kinetic energy of eddies in a spectral range from large (shear scale) to small (wake scale) scales, as also considered by Liu et al. (1996). However, this approach may complicate the parameterisation of the different TKE transfer terms inside the canopy. The energy spectra of the flow provides details of the fine structures of the turbulence within the canopy, but this is better documented for vegetation canopies than for urban canopies. Thus, our adaptation of the TKE equation to urban canopy (building canopy or canopy with buildings and vegetation) is largely an extension of the previous studies done for vegetated canopies. The energy spectra of a flow within a building and vegetation canopy is probably more complex than a strictly vegetated canopy because of the differences of size and volume between buildings and vegetation.

Similar to the momentum equation, the interaction of the airflow with buildings and vegetation is considered by including additional source and/or sink terms in the equation for TKE:

$$\frac{\partial E}{\partial t} = \underbrace{-\frac{\partial \langle u_i \rangle E}{\partial x_i}}_{[1]} + \underbrace{\left\{ K_m \left[\left(\frac{\partial \langle u_x \rangle}{\partial z} \right)^2 + \left(\frac{\partial \langle u_y \rangle}{\partial z} \right)^2 \right] S_{\text{air}} + F_E^{\text{bui}} \right\}}_{[2]}$$

$$+ \underbrace{\left\{ \frac{g}{\theta_v} \langle w\theta_v \rangle + H_E \right\}}_{[3]} \underbrace{- \frac{1}{\rho} \frac{\partial (\rho \langle wE \rangle)}{\partial z}}_{[4]} \underbrace{- \varepsilon}_{[5]} + \underbrace{\sum_j W_E^j}_{[6]} \underbrace{- \sum_j D_E^j}_{[7]}, \tag{14}$$

where E is the TKE, θ_v is the virtual potential temperature, g is the gravity acceleration, and K_m is the eddy diffusivity for momentum. The terms on the right-hand side of Equation (14) represent, respectively, the advective transport term by the mean flow, the dynamic shear production term, the buoyancy production term, the turbulent transport term, the turbulent dissipation term, the TKE accelerated cascade term, and the wake production term. The dissipation rate ε of TKE is estimated from the dissipation time scale τ_0 ($\varepsilon = E\tau_0^{-1}$), which depends on the turbulent length scale. The vertical TKE flux $\langle wE \rangle$ and τ_0 are assessed following Ballard et al. (1991).

The presence of the horizontal building surfaces creates friction forces on the wind flow inducing a TKE shear production. Thus, in Equation (14), the total shear production term [2] is divided into two parts. The first part of [2] corresponds to the dynamic shear production by the mean flow. The second part corresponds to the shear production by the building horizontal surfaces, which is parameterised from the friction velocity and the eddy diffusivity K_m for momentum:

$$F_E^{\text{bui}}(k) = \frac{f_{\text{bui}} \text{Surf}_{\text{bui}} [u_{*\text{bui}}(k)]^4}{K_m(k)}. \tag{15}$$

The sensible heat fluxes emitted from buildings and vegetation, D_θ (Equation (10)), and the anthropogenic heat fluxes, A_θ (Equation (11)), are considered through the buoyancy production term [3], which corresponds to the conversion of potential energy to TKE:

$$H_E(k) = \frac{g}{\theta_v(k)} V_{\text{air}}(k) [D_\theta(k) + A_\theta(k)]. \tag{16}$$

Without a canopy, the transfer of energy (i.e., cascade of energy) across the inertial subrange of the spectra (i.e., from large-scale to Kolmogorov scale eddies) is assumed by the Kolmogorov theory to be independent of the eddy size and equal to the dissipation rate ε. As explained by Finnigan (2000), within a vegetation canopy

two additional effects modify the inertial subrange part of the spectra, making the Kolmogorov theory inapplicable.

First, the work against the pressure drag of the foliage converts the kinetic energy of the mean flow into fine scale turbulence (wakes) and into heat for the work against the viscous drag of the foliage. The wake production of TKE is due to the interaction between the mean flow and the canopy elements, and is represented in our model by the conventional parameterisation used for the vegetation canopies extended to the buildings:

$$W_E^j(k) = C_{dj} A_{fj}(k)(\langle u_x \rangle^2 + \langle u_y \rangle^2)^{1.5}. \tag{17}$$

Second, by interacting with the foliage, the eddies larger than the canopy elements lose their TKE to heat and wake kinetic energy, which represents a continuous removal of energy from the eddy cascade violating the Kolmogorov theory, referenced as a spectral shortcut between large and small eddy scales compared to the inertial transfer. In another way, the large eddies are broken by the canopy elements, which induces smaller eddies that accelerate the TKE dissipation by their presence. All measurements within a vegetation canopy show that turbulent eddies roll-off considerably faster than the Kolmogorov theory would predict (Finnigan, 2000). To consider the accelerated cascade of TKE from large to small scales due to the presence of the vegetation compared to the energy cascade parameterised by the Kolmogorov theory (turbulent dissipation rate), Green (1992) and Liu et al. (1996) added to the TKE equation a sink term that we extend to the building canopy. This term is represented by Equation (18) below. As also observed by Liu et al. (1996), without this last term, the turbulent dissipation is underestimated compared to the TKE production,

$$D_E^j(k) = 4C_{ij} A_{fj}(k)(\langle u_x \rangle^2 + \langle u_y \rangle^2)^{0.5} E(k). \tag{18}$$

The turbulent dissipation rate is probably the most delicate term to parameterise inside the canopy because it is not constant between large and Kolmogorov eddy scales as it is above the canopy. Because our TKE considers large and small eddies, the TKE dissipation rate may just be an approximation. For simplification, the same parameterisation as the one above the canopy is used for the dissipation of the large eddies where a correction term has been added in the TKE equation through the Equation (18) to consider the modification of the Kolmogorov theory induced by the interaction between large eddies and the canopy elements. For the small-eddy production from the mean flow interaction with buildings and vegetation, their dissipation rate is assumed to follow the Kolmogorov theory with a smaller TLS. This additional contribution to dissipation is considered by introducing an additional length scale within the canopy to the current TLS (see next section). This parameterisation of ε is an operational expediency because we use the same TKE for the dissipation rate of large and small eddies; it seems to us that it is a practical way to simulate a correct equilibrium within the canopy between the

different TKE budget components (see Subsection 6.1) without splitting the TKE equation. In the Subsection 6.6, we show that the introduction of an additional TLS ameliorates the effect of discontinuity in the profile of the eddy diffusivity between the inside and the outside of the canopy by controlling the exchanges between the canopy and the free atmosphere.

3.5. TURBULENT LENGTH SCALE

In the GSPBL scheme of MM5, the parameterisation of the TLS, l, used to assess τ_0 and the eddy diffusivities has been changed because an underestimation of the mixing inside the PBL during convective conditions has been observed, which is one of the problems of the local closure turbulence schemes (Bélair et al., 1998), such as GSPBL. The TLS parameterisation of Bougeault and Lacarrère (1989) is now used during stable and unstable conditions inside the PBL. This parameterisation includes a non-local feature in the parameterisation of the eddy diffusivity. The mixing length l_{BL} is derived from the upward and downward displacements (l_{up} and l_{down}) that could be achieved by parcels having kinetic energy equal to the mean TKE before being stopped by buoyancy effects. l_{up} and l_{down} are determined from the following equations:

$$\int_{z}^{z+l_{\text{up}}} \frac{g}{\theta_{vs}}[\theta_v(z') - \theta_v(z)]dz' = E(z) \tag{19a}$$

and

$$\int_{z-l_{\text{down}}}^{z} \frac{g}{\theta_{vs}}[\theta_v(z) - \theta_v(z')]dz' = E(z), \tag{19b}$$

where $l_{\text{down}} < z$, and θ_{vs} is the virtual potential temperature near the surface.

Here, l_{BL} is deduced by averaging l_{up} and l_{down} as proposed by Bélair et al. (1999):

$$\frac{1}{l_{\text{BL}}} = \frac{1}{2}\left(\frac{1}{l_{\text{up}}} + \frac{1}{l_{\text{down}}}\right). \tag{20}$$

Thus, above the canopy, $l = l_{BL}$.

Inside the canopy, the TLS is more complex due to the effects of canopy elements, which break the large eddies when they penetrate inside the canopy, and which create small eddies from their interaction with the mean flow. Following Martilli et al. (2002), a new length scale is added within the canopy to account for the eddies generated by buildings, which is extended here to the vegetation:

$$\frac{1}{l(k)} = \frac{1}{l_{\text{BL}}(k)} + \frac{1}{l_{\text{can}}(k)}, \tag{21}$$

where l_{can} is the new TLS induced by the canopy elements.

l_{can} takes into account at the level k of eddies induced by higher canopy elements:

$$\frac{1}{l_{can}(k)} = \sum_{p=k}^{k_{top}} \frac{\sum_j f_j \mathrm{Surf}_j(p)}{[1 - \mathrm{Surf}_{tot}(0)]} \frac{1}{z(p)}, \tag{22a}$$

for $\mathrm{Surf}_{tot}(0) \neq 1$, and

$$1/l_{can}(k) = 0, \tag{22b}$$

for $\mathrm{Surf}_{tot}(0) = 1$.

4. Description of the SM2-U(3D) Model

Initially, the soil model SM2-U determines the mean canopy surface temperature and mean heat fluxes at the canopy-atmosphere interface for the lower boundary condition of atmospheric models using the RA. SM2-U is an extension of the rural soil model ISBA (Noilhan and Planton, 1989) to urban surfaces, thus it considers in detail both rural and urban surfaces. The building wall effects are included through the equation of the paved surface temperature by introducing the heat stored by building walls, and by modelling the radiative trapping with an effective street canyon albedo parameterisation deduced from Masson (2000). Thus, for dense urban districts, the paved surfaces are assimilated to street canyons; their temperature and heat fluxes correspond, respectively, to an effective mean temperature of street canyon surfaces and to mean heat fluxes at the top of street canyons.

Three soil layers are considered by SM2-U (see Figure 1): a surface soil layer for the natural surfaces, allowing the evaluation of the evaporation fluxes from the bare soil; a root zone layer representing the influence area of the vegetation roots; and a deep soil layer used as a water reservoir to provide water to the root zone layer by diffusion in dry periods. SM2-U also determines the water intercepted by the canopy elements by representing the roofs, the paved surfaces and the vegetation by a water reservoir. The model is thus capable of simulating the surface water runoff. More details on SM2-U can be found in Dupont (2001).

With the DA, the new version of SM2-U, called SM2-U(3D), assesses at each level inside the canopy the heat fluxes (sensible and latent) from the canopy elements and the water intercepted by the canopy elements. The ground part in SM2-U(3D) (i.e., the soil layer water content and the ground surface heat flux equations) is identical to SM2-U.

The modifications of the hydrological representation of roofs and vegetation are not described in this paper because the model is not applied for a rainy event. But

with the DA, the roofs and vegetation water reservoirs are vertically distributed following the surface vertical distribution. Thus, the equations of evolution of the water intercepted by these reservoirs are solved at each level inside the canopy.

4.1. MEAN HEAT FLUXES INSIDE THE CANOPY

The mean surface heat fluxes Φ_{mean} emitted at the level k per unit of ground (W m^{-2}) are computed from:

$$\Phi_{\text{mean}}(k) = \sum_j f_j \text{Surf}_j(k) \Phi_j(k) + f_{\text{pav}} \Phi^*_{\text{pav}}(k), \tag{23}$$

with $j \in \{\text{bare, bui, nat, vega, vegn, wat}\}$ and Φ represents either the net radiation flux (R_n), the sensible heat flux (H_{sens}), the latent heat flux (LE), or the storage heat flux (G_s). The superscript * indicates that the variable has been modified from the initial parameterisation to consider the heat repartition inside the street canyons, which is described in Subsection 4.3.

The parameterisations of the surface temperatures and of the sensible and latent heat fluxes are similar to those used in SM2-U but extend to all levels inside the canopy (see Appendix B).

4.2. NET RADIATION FLUX

The surface net radiation parameterisation in SM2-U(3D) is similar to the one used in SM2-U but extended to all levels inside the canopy, and attenuated by the presence of the taller canopy elements. As initially used for vegetation canopy, and extended by Brown (2000) to the urban canopy, the net radiation within the canopy is assumed to exponentially decay toward the ground. It corresponds to an approximation of Beer's law, which is initially valuable for the attenuation of parallel monochromatic radiation through a homogenous medium, viz.

$$\begin{aligned} R_{nj}(k) \;=\; & [(1-\alpha_j) R_G(k_{\text{top}}) - \varepsilon_j \sigma (T_{sj}(k)^4 - \varepsilon_a T (k+1)^4)] \\ & \times \exp\left[\frac{-k_{\text{ex}} \sum_{p=k+1}^{k_{\text{top}}} \left[\sum_i f_i A_{pi}(p) \right] \Delta z(p)}{|\cos Z_e|} \right], \end{aligned} \tag{24}$$

where j and $i \in \{\text{bare, bui, nat, pav, vega, vegn, wat}\}$, R_G is the direct and diffused solar radiation, σ the Stefan-Boltzmann constant, α_j and ε_j the surface albedo and emissivity, ε_a and T the air emissivity and temperature, $k_{\text{ex}} = 1.5$ the radiation extinction coefficient, which can be reasonably assumed constant over any wavelength band (Hamlyn, 1992), and Z_e the zenith angle.

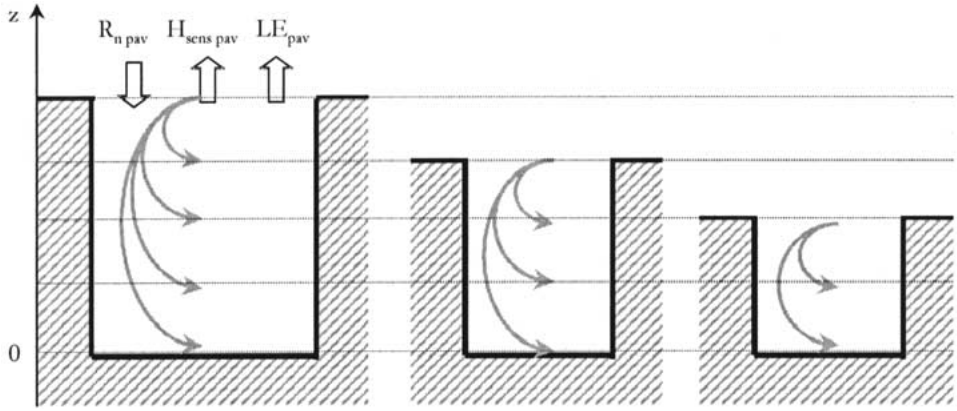

Figure 2. Scheme of the vertical distribution inside the street canyon of heat fluxes assessed at the top of the street for the different streets inside a computational cell.

4.3. HEAT FLUXES FROM PAVED SURFACES

In SM2-U(3D), the heat fluxes from paved surfaces correspond for dense urban districts to heat fluxes from the top of the street canyons as in SM2-U. The assimilation of paved surfaces to street canyons is quite easy with the RA because the thickness of the first computational layer is definitely larger than the canopy thickness. With the DA, the heat fluxes from the street canyons, $R_{n\,\mathrm{pav}}$, $H_{\mathrm{sens\,pav}}$ and LE_{pav} (where L is the latent heat of vaporization), are assessed, respectively, through the paved surfaces' Equations (24), (B4) and (B8), by considering a vertical distribution of the tops of the street canyons. These fluxes are after vertically distributed inside the street, and are denoted $R^*_{n\,\mathrm{pav}}$, $H^*_{\mathrm{sens\,pav}}$ and LE^*_{pav}.

The latent heat flux is considered as emitted at the floor level, the water interception by walls being neglected. Thus,

$$LE^*_{\mathrm{pav}}(k) = 0, \tag{25a}$$

and

$$LE^*_{\mathrm{pav}}(0) = \sum_{p=0}^{k_{\mathrm{top}}} \mathrm{Surf}^*_{\mathrm{pav}}(p) LE_{\mathrm{pav}}(p), \tag{25b}$$

where $\mathrm{Surf}^*_{\mathrm{pav}}$ is the top area density of the street canyon.

The sensible and net radiative fluxes assessed at the top of the street canyons are distributed inside the street following the sky view factor of the walls and of the street floor (see Figure 2). For one street canyon having its top at level p, the heat flux at level k $(0 < k < p)$ is:

$$\phi^*_{\mathrm{pav}}(k) = \frac{2\Delta z(k)\Psi_{w\to s}(p,k)}{\sum_{t=1}^{p-1}[2\Delta z(t)\Psi_{w\to s}(p,t)] + W(p)\Psi_{r\to s}(p,0)}\phi_{\mathrm{pav}}(p), \tag{26a}$$

and the heat flux at the ground level is:

$$\phi^*_{\text{pav}}(0) = \frac{W(p)\Psi_{r\to s}(p,0)}{\sum_{t=1}^{p-1}[2\Delta z(t)\Psi_{w\to s}(p,t)] + W(p)\Psi_{r\to s}(p,0)}\phi_{\text{pav}}(p), \tag{26b}$$

where $\phi \in \{H_{\text{sens}}, R_n\}$, $\psi_{r\to s}(p,0)$ is the sky view factor from the street canyon floor having its top at the level p, $\psi_{r\to s}(p,k)$ the sky view factor at the level k from one wall of the street canyon having its top at the level p, and $W(p)$ is the width of the street canyon having its top at the level p.

To account for a vertical distribution of street canyons, the contributions at the level k of the higher street canyons having their tops between the levels $k+1$ and k_{top} are considered by modifying the Equations (26) as:

$$\phi^*_{\text{pav}}(k) = \sum_{p=k+1}^{k_{\text{top}}}\left[\frac{2\text{Surf}^*_{\text{pav}}(p)\Delta z(k)\Psi_{w\to s}(p,k)}{\sum_{t=1}^{p-1}[2\Delta z(t)\Psi_{w\to s}(p,t)] + W(p)\Psi_{r\to s}(p,0)}\phi_{\text{pav}}(p)\right] \tag{27a}$$

and

$$\phi^*_{\text{pav}}(0) = \sum_{p=1}^{k_{\text{top}}}\left[\frac{\text{Surf}^*_{\text{pav}}(p)W(p)\Psi_{r\to s}(p,0)}{\sum_{t=1}^{p-1}[2\Delta z(t)\Psi_{w\to s}(p,t)] + W(p)\Psi_{r\to s}(p,0)}\phi_{\text{pav}}(p)\right] + \text{Surf}^*_{\text{pav}}(0)\phi_{\text{pav}}(0). \tag{27b}$$

To assess the width of the street canyons and the sky view factors, it is assumed that (i) all buildings are parallelepipeds with the same square horizontal section characterized by their area S_{bui}, (ii) all buildings are surrounded by paved surfaces (i.e., street canyons), and (iii) each street canyon has a constant width with the height. Thus, the mean width of the street canyons having a height equal to $z(p)$ is:

$$W(p) = \frac{\text{Surf}^*_{\text{pav}}(p)(S_{\text{bui}})^{0.5}}{2\text{Surf}_{\text{bui}}(p)}. \tag{28}$$

The calculations of the sky view factors are adapted from Masson (2000):

$$\psi_{r\to s}(p, k=0) = \left[\left(\frac{z(p)}{W(p)}\right)^2 + 1\right]^{0.5} - \frac{z(p)}{W(p)}, \tag{29}$$

and

$$\psi_{w\to s}(p,k) = \frac{1}{2}\left\{\frac{z(p)-z(k)}{W(p)}+1-\left[\left(\frac{z(p)-z(k)}{W(p)}\right)^2+1\right]^{0.5}\right\} \times\left(\frac{z(p)-z(k)}{W(p)}\right)^{-1}. \quad (30)$$

5. Model Application

The new MM5 version, DA-SM2-U, is tested for Philadelphia, in Pennsylvania, U.S.A., on 14 July 1995, a day characterized by anticyclonic conditions, abundant sunshine and high temperatures, and largely stagnant conditions on the eastern United States and southern Canada. MM5 Version 3, Release 5 was run in a one-way nested configuration for several days in July including five nested MM5 computational domains with 108-, 36-, 12-, 4-, and 1.33-km horizontal grid spacing. DA-SM2-U is used only on the 1.33-km domain. To compare DA-SM2-U with RA MM5 versions, two other simulations using RA are performed: a 'standard' version of MM5 (hereafter, RA-SLAB), and a 'standard' version of MM5 coupled with SM2-U (hereafter, RA-SM2-U). These last two simulations use 30 vertical layers, and the anthropogenic heat fluxes are considered as in DA-SM2-U to focus the thermodynamic comparisons on the soil model parameterisations. For DA-SM2-U, ten layers were added in the lowest 100 m (lowest layer depth of 4 m) in comparison to RA simulations to resolve flow within the rural and urban canopies.

These three MM5 versions use the GSPBL model including the parameterisation of the TLS of Bougeault and Lacarrère (1989) inside the PBL (described in sub-Section 3.5.). In RA-SLAB, there is a single urban category defined from U.S. Geological Survey (USGS) 24-category database. For RA-SM2-U and DA-SM2-U versions, seven urban sub-categories have been roughly constructed inside the USGS to cover the urban area following Ellefsen (1990–1991), as represented in Figure 3. Each of these urban sub-categories is characterized by the surface density of buildings and paved surfaces, by the building mean height and by a roughness length used by the RA versions (see Table I). All physical properties of artificial surfaces are the same in each urban sub-category: buildings are represented with concrete walls and roof, and with a horizontal section S_{bui} = 100 m^2; and paved surfaces are made with asphalt. For DA-SM2-U, the vertical distributions of buildings and vegetation have been constructed following their average height and the shaped profiles indicated in Figure 4. A mean vegetation height has been assigned for each of the USGS categories. It is assumed that the vertical distribution of the street canyon tops is identical to the roof vertical distribution, i.e., $\mathrm{Surf}^*_{\mathrm{pav}}$ =

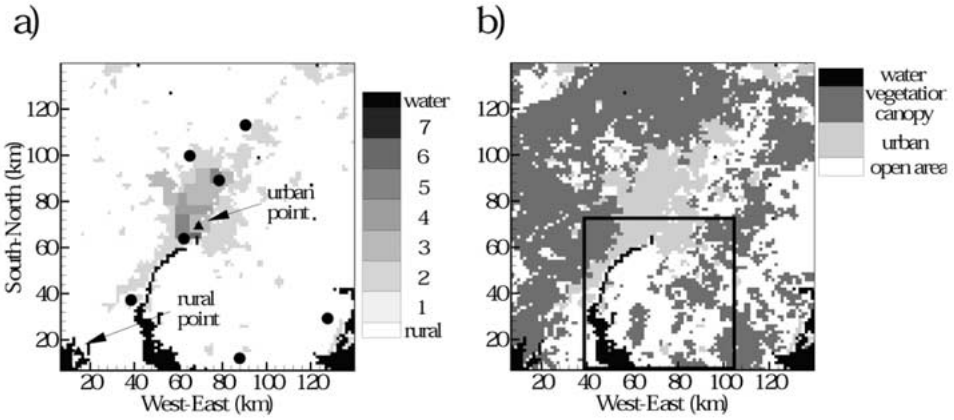

Figure 3. The 1.33-km domain centered on Philadelphia. The box in the southern end of the domain delineates the area shown in Figure 18a. (a) The seven urban categories, with the positions of the rural and urban points (black triangles) where the vertical profiles are analysed, and of the seven surface observation stations (black circles). (b) Principal land-use categories, the open areas corresponding to the rural surfaces with small vegetation.

TABLE I

Main characteristics of the seven urban categories.

Urban categories	Mean building height $h_{\text{bui mean}}$ (m)	Roof fraction of the artificial surfaces $f_{\text{bui}}(f_{\text{bui}} + f_{\text{pav}})^{-1}$	Roughness length (m)
1	4.5	0.30	0.70
2	7.0	0.30	1.10
3	8.0	0.40	1.00
4	4.0	0.10	0.20
5	7.0	0.15	0.35
6	32.0	0.60	1.50
7	64.0	0.15	3.20

Surf_{bui}. The building plan and frontal area density, respectively $A_{p\text{bui}}$ and $A_{f\text{bui}}$, are deduced from the roof area density by considering that the roof area is equal to the building section area, which is assumed vertically constant. In the next section, the DA-SM2-U simulation is referenced as the base simulation.

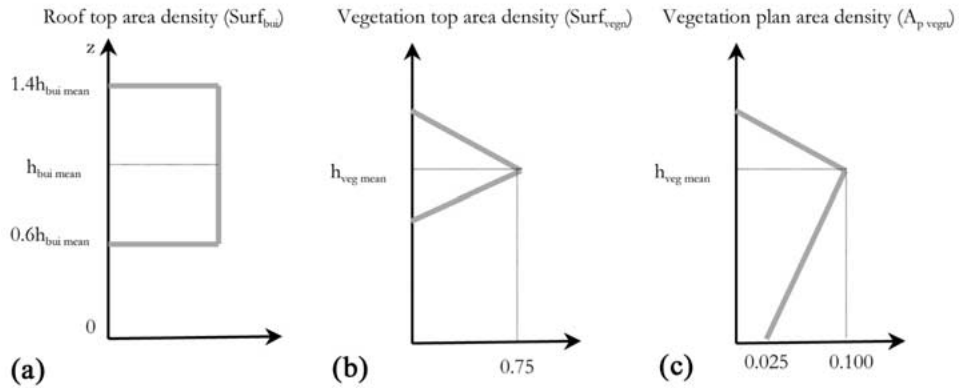

Figure 4. Shape profiles used for describing (a) the roof area density, (b) the vegetation area density, and (c) the vegetation plan area density. $h_{\mathrm{bui\,mean}}$ is the mean height of the building defined for each urban category, and $h_{\mathrm{veg\,mean}}$ is the mean height of the vegetation defined for each vegetation category.

6. Analyses of the Vertical Profiles inside the RSL

In this section, the behaviour of the DA-SM2-U simulation inside the RSL is analysed through the dynamic, turbulent, thermal, and humidity vertical profiles above a rural and an urban point indicated in the Figure 3a. These two points are, respectively, characterized by a 20-m tall vegetation canopy and a 45-m tall building canopy. The correct simulation of these profiles within and above the canopy is important because primary atmospheric pollutants are emitted inside the RSL and thus the first chemical reactions and dispersion, which occur in this layer, depend on the meteorological fields.

6.1. TKE BUDGET COMPONENTS

Figure 5 represents the normalized vertical profiles of the TKE budget components for the rural (a) and urban (b) points at 1400 local time. The shape and magnitude of these profiles inside the vegetation and building canopies are very close despite the difference of the canopy element vertical distribution, and even though the same approach to represent the effect of the vegetation and of the buildings has been used. The shear and wake terms correspond to a production term of TKE, and they are characterized by a maximum value in the upper part of the canopy. These peaks are at the same altitude for the vegetation, in agreement with Raupach et al. (1986), whereas the shear peak is slightly higher for the building canopy, which is probably explained by the difference in vertical distribution between buildings and vegetation. The shear production is very small in the lower two-thirds of the canopies, which is consistent with Leclerc et al. (1990) in a vegetation canopy where the wake production and turbulent transport terms approximately balance the dissipation term. The turbulent transport term is a sink for TKE at the canopy top

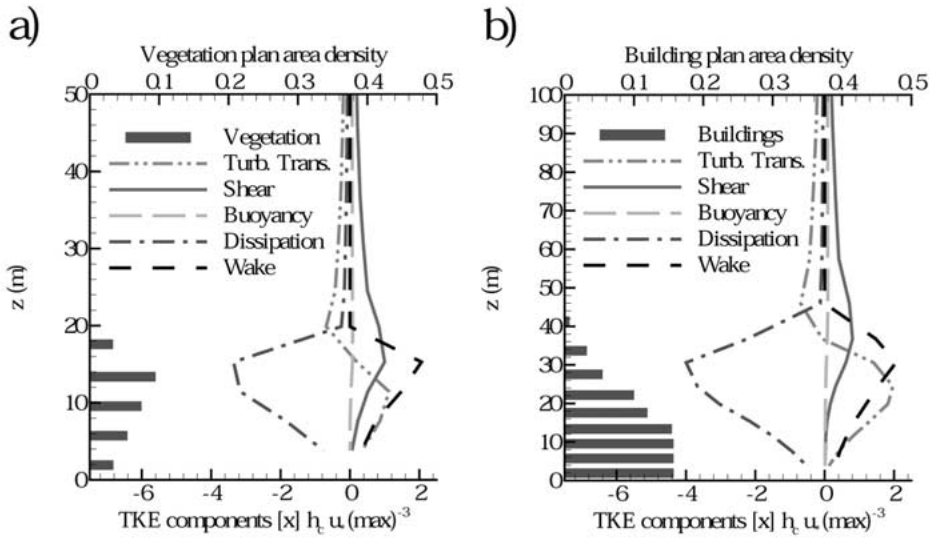

Figure 5. Normalized vertical profiles of the budget of the turbulent kinetic energy at 1400 local time for (a) a rural and (b) an urban point. h_c is the local height of the canopy and u_*(max) is the maximum friction velocity. The vegetation and building area densities indicate the canopy structure. Note that the dissipation term corresponds to the sum of the term [5] and [7] in Equation (14).

and an important source in the lower canopy, which means that TKE is imported inside the canopy from above, corresponding to the penetration of large eddies inside the canopy that maintains a significant TKE level in the lower canopy. The dissipation term is maximized at the same level as the shear and wake terms but remains significant in the lower part of the canopy. This dissipation is composed of two terms: (i) ε, the dissipation term of large eddies, and small eddies from the wake production, and (ii) D_E^j (Equation (18)), the dissipation term due to the TKE accelerated cascade. The buoyancy term corresponds to a TKE production term, which means that the heat flux is positive. It is negligible in the lower portion of the canopy, whereas near the top of the canopy it is near 12% and 14% of the shear production, respectively for the rural and urban canopies, and 25% at 20 m above the canopies. With the LES model of Shen and Leclerc (1997), the buoyancy term is less than 10% of the shear production near the vegetation canopy top.

The general features of the TKE vertical components in the rural RSL agree very well with simulations and observations reported in the literature for the vegetation canopies. For the urban RSL, our TKE budget terms are slightly different from those simulated by the model of Ca et al. (2002) for very unstable stratification. Their model simulates a very strong wake production at the top of the canopy, which decreases rapidly inside the canopy, the buoyancy production term is larger than ours, especially in the lower part of the canopy, and their turbulent transport term is a TKE source above the canopy, a sink just below and a source for the last part of the canopy. Unfortunately, as far as we are aware, there are no available

measurements of the TKE budget components inside an urban canopy, and it is thus difficult to quantify the quality of the results.

6.2. TKE

In Figure 6a, the TKE profile simulated by DA-SM2-U at 1400 local time inside the RSL is compared with those simulated by RA cases for the urban and rural points. The DA-SM2-U TKE profile increases inside the canopy with height with a subtle maximum just above the vegetation canopy, whereas TKE continues to increase above the urban canopy toward a quasi-constant value due to the stronger mixing inside the PBL. The TKE maximum induced by the shear production is more pronounced overnight at the top of the rural and urban canopies (not shown) because of the lower mixing inside the PBL. This TKE maximum has also been observed in near-neutral conditions by Kastner-Klein (2001) and Rotach (1995) for modelled and real urban canopies, and Brunet et al. (1994) for a modelled vegetation canopy. Martilli et al. (2002) have also simulated the same diurnal behaviour of the TKE profiles above an urban canopy, which is in agreement with measurements. However, the maximum values of the TKE profiles normalized by $u_*(\max)^2$ seem too low compared to the measurements made in urban canopies by Rotach (1993), Oikawa and Meng (1995) and Louka et al. (2000), and in a modelled vegetation canopy by Brunet et al. (1994). DA-SM2-U simulates a maximum value around 1.5 whereas measurements seem to indicate values between 3 and 6. These low values simulated by DA-SM2-U may be explained by the fact that they correspond to horizontal average values on a 1.3×1.3 km^2 grid cell inside an heterogeneous canopy; they are thus representative of a small district with different levels of roof and vegetation, whereas measurements are made in one particular location inside a street canyon or inside a homogeneous vegetation canopy. The RA-SLAB and RA-SM2-U TKE profiles are similar for both canopies; TKE increases with height to reach a quasi-constant value at 200 m.

6.3. Shear stress

The DA-SM2-U local shear stress u_* normalized by its maximum value $u_*(\max)$ at 1400 local time (Figure 6b) is characterized by a maximum near the top of the canopy and a decrease toward the ground inside the canopy. For the RA cases, the profiles start near the top of the canopy and are very close to the shape of the DA-SM2-U profile. The same behaviour of the normalized u_* profile as in DA-SM2-U has been observed in real canopies and modelled wind-tunnel canopies (see, for example, Rotach (1995) and Kastner-Klein (2001) for urban canopies and Raupach et al. (1996) for vegetation canopies). Kastner-Klein observed a negligible momentum flux in the lower part of canopies with a large building density that is not really simulated in our case. The maximum value of u_* is achieved at the top of the vegetation canopy, which is in agreement with previous studies (cf. Shen and Leclerc, 1997), but for the urban canopy this maximum is somewhat lower than

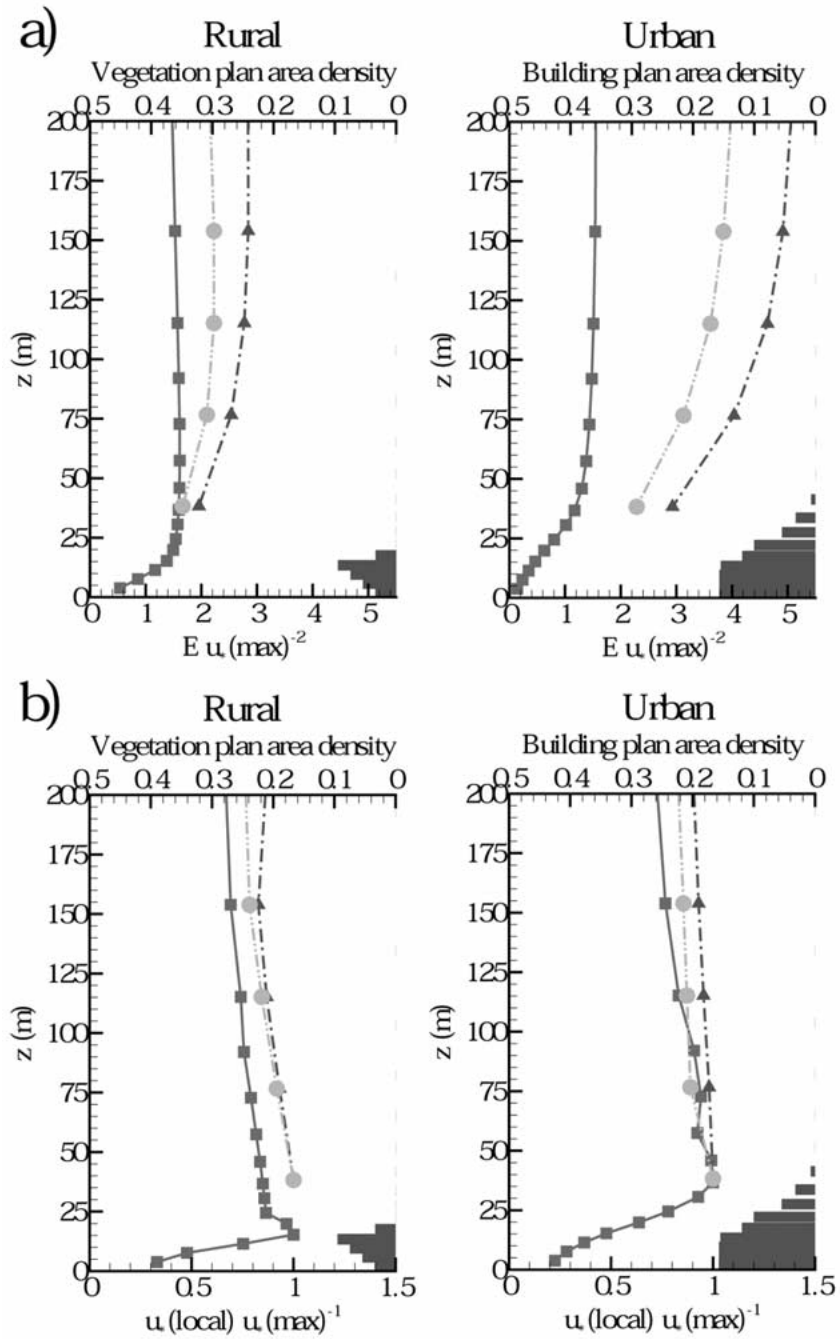

Figure 6. Vertical profiles for a rural and an urban point of (a) the turbulent kinetic energy normalized by $u_*(\max)^2$ and of (b) the local u_* normalized by its maximum value $u_*(\max)$, at 1400 local time, for the three MM5 versions: RA-SLAB (dashed dot dot line with circles), RA-SM2-U (dashed dot line with triangles) and DA-SM2-U (solid line with squares).

that shown by measurements and other modelling studies, it is situated generally between 1.5 to 2 times the mean height of the canopy. In our case, the maximum is just above the mean building height but it depends probably on the building vertical morphology.

6.4. Potential air temperature

From the vertical profiles of the potential air temperature above the rural and urban areas (Figure 7), it seems that DA-SM2-U simulates a neutral layer during the night up to 75 m above both canopies, and neutral and unstable stratification within the rural and urban canopies respectively. RA-SM2-U simulates the same neutral layer but only above the urban area; a stable layer is simulated above the rural area. RA-SLAB simulates a colder urban neutral layer. The urban neutral layer is consistent with the observed reduction of atmosphere stability near urban surfaces (Roth, 2000). As in Martilli et al. (2002), the depth of the neutral layer is in agreement with values given by Oke (1995). The neutral layer above the vegetation canopy with DA-SM2-U is unexpected, and seems slightly too large for a point upstream of the city. It is probably explained by the larger values of TKE at the top of the canopy that increase the TLS, and thus increase the mixing above the vegetation canopy. Inside the urban canopy, the air is constantly warmer than the air in the upper part of the RSL as observed by Rotach (1995) in a street canyon of Zurich. Inside the vegetation canopy, the air has near-neutral stratification during the night and slightly unstable during the day, whereas Kaimal and Finnigan (1994) report that the typical air stratification is unstable during the night and stable during the day. Ni (1997) reports a sigmoid-shaped potential air temperature profile within the forest canopy during the day, with local maxima at the level of the maximum foliage density and near the ground because of the solar radiation absorption by the canopy elements and the ground surface. He also noted that if the vegetation canopy is sparse, then the global maximum potential temperature is at the ground surface. In our case, the unstable stratification observed within the vegetation canopy during the day could be explained by a sparse canopy, but probably more by a too small vertical resolution of the meteorological fields within the vegetation canopy.

6.5. Air specific humidity

The air specific humidity (q_v) profiles (Figure 8) above the rural area have a similar shape to the potential air temperature profiles, except that q_v decreases with height above the RSL. The humidity is constant inside the vegetation canopy, larger than above the canopy during the day because of the vegetation transpiration. The rural humidity profiles simulated with the RA are similar to DA-SM2-U during the day. During the night, as a consequence of the larger mixing above the rural canopy with DA-SM2-U, q_v is nearly constant from the canopy top to 100 m. The RA-SM2-U and DA-SM2-U urban q_v is quasi constant inside the RSL with smaller values than above the rural area. No discontinuity in the DA-SM2-U profile is

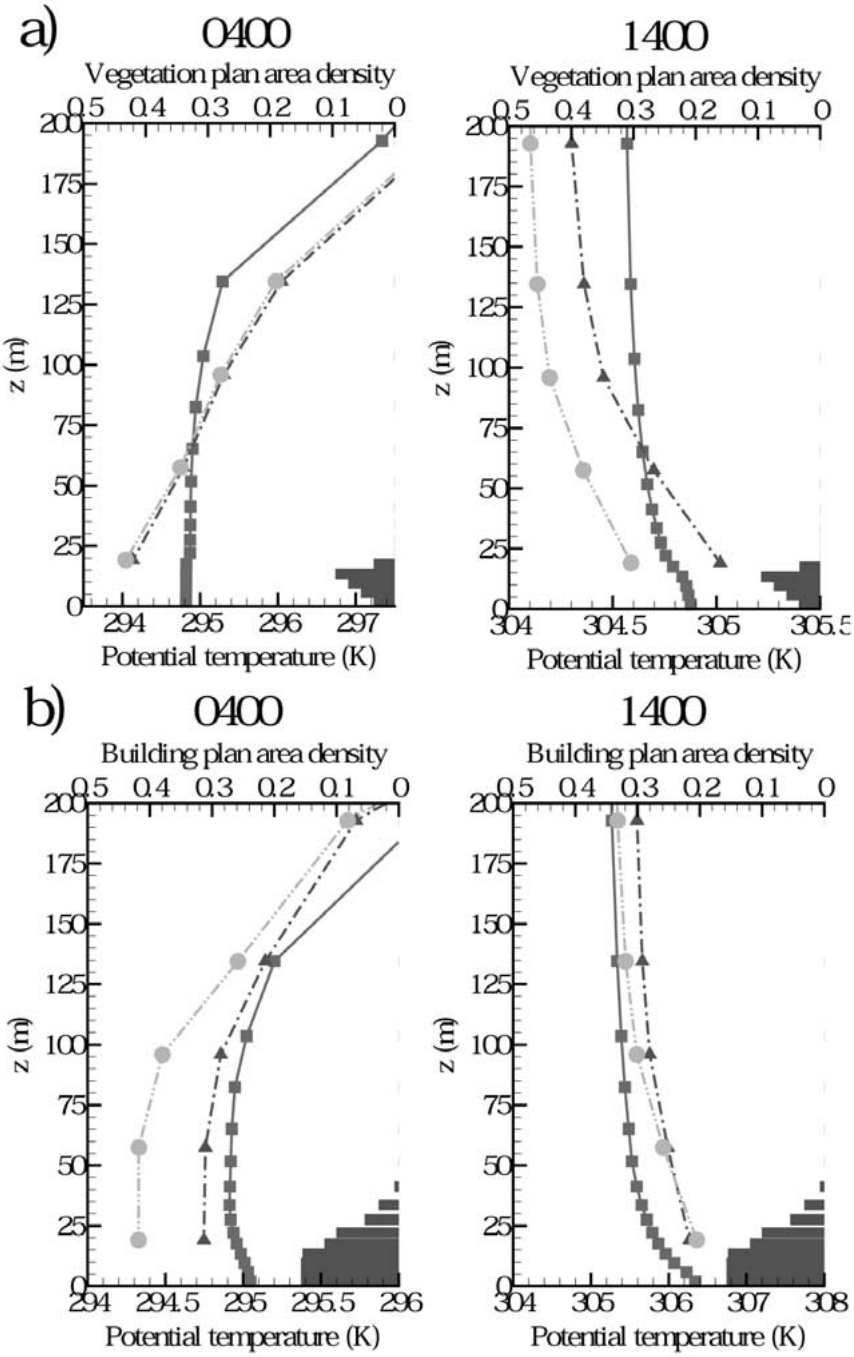

Figure 7. Vertical profiles of the potential air temperature for (a) a rural and (b) an urban point at 0400 and 1400 local time, for the three MM5 versions: RA-SLAB (dashed dot dot line with circles), RA-SM2-U (dashed dot line with triangles) and DA-SM2-U (solid line with squares).

observed between the inside and the outside of the canopy because no water vapour is emitted from urban surfaces. The profiles simulated by the cases using SM2-U are close above the urban area whereas the one from RA-SLAB is characterized by larger q_v values and a maximum near the ground. As discussed in the sub-Section 7.2., RA-SLAB simulates a non-negligible latent heat flux from urban surfaces.

6.6. EDDY DIFFUSIVITY

The eddy diffusivity is an important prognostic variable for atmospheric and air-quality modelling because it controls the vertical mixing of meteorological and pollutant quantities. Figure 9 compares the eddy diffusivity K_h for heat inside the RSL simulated by the three MM5 versions at 0400 and 1400 local time for the urban and rural points. The nocturnal K_h is characterized by a peak just above the canopies before decreasing inside the canopy and reaching a near zero value in the lower half of the canopy. The K_h peak seems too high, and is due to the large value of TKE and to the neutral stratification at the top of the canopies, which increases the mixing inside the RSL, with little mixing in the stable stratification of the upper atmospheric layers. With both RA versions, the nocturnal K_h peaks are not simulated. During the day, the DA-SM2-U K_h profile and K_h values are very similar to the night hours inside the canopy. The strong profile discontinuity observed between the inside and the outside of the canopies has also been reported by Denmead (1964) and Finnigan (2000) in vegetation canopies. Above the canopy, the mixing being larger inside the thicker PBL, K_h increases with height to reach a maximum in mid-regions of the PBL as also with the RA cases (not shown). The RA K_h profiles seem to tend to a zero vertical gradient near the canopy top.

To study the impact of the TLS parameterisation on the eddy diffusivity, two modified DA-SM2-U simulations are performed. In the first simulation (hereafter, sim1), the TLS parameterisation is not modified inside the canopy, i.e., $l = l_{BL}$; and in the second (sim2) the upward and downward displacement length scales, l_{up} (Equation (19a)) and l_{down} (Equation (19b)), are limited respectively inside and outside the canopy to decrease the penetration of the large eddies inside the canopy. Hence,

$$\text{for } k > k_{\text{top}}, l_{\text{down}} \leq z(k) - z(k_{\text{top}}),$$

and

$$\text{for } k \leq k_{\text{top}}, l_{\text{up}} \leq z(k_{\text{top}}) - z(k).$$

In Figure 10, the K_h profiles from sim1 and sim2 for the rural and urban points at 0400 and 1400 local time are compared with the K_h profile from the base simulation. Without changing the TLS inside the canopy (sim1), the nocturnal K_h profile has the same shape as the reference one with a larger maximum above the urban canopy. The sim1 nocturnal profile discontinuity induced by the

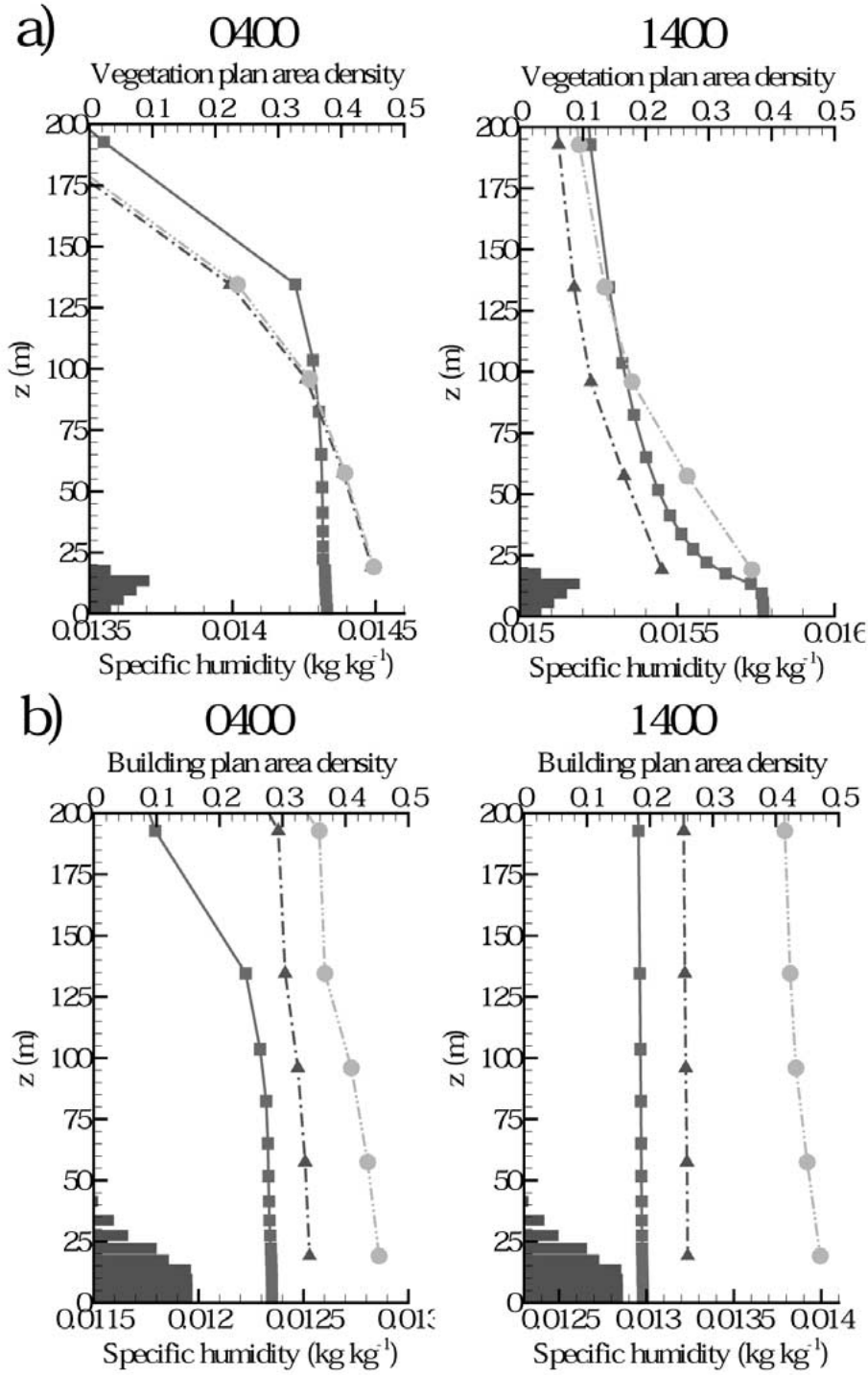

Figure 8. As in Figure 7, but for the air specific humidity.

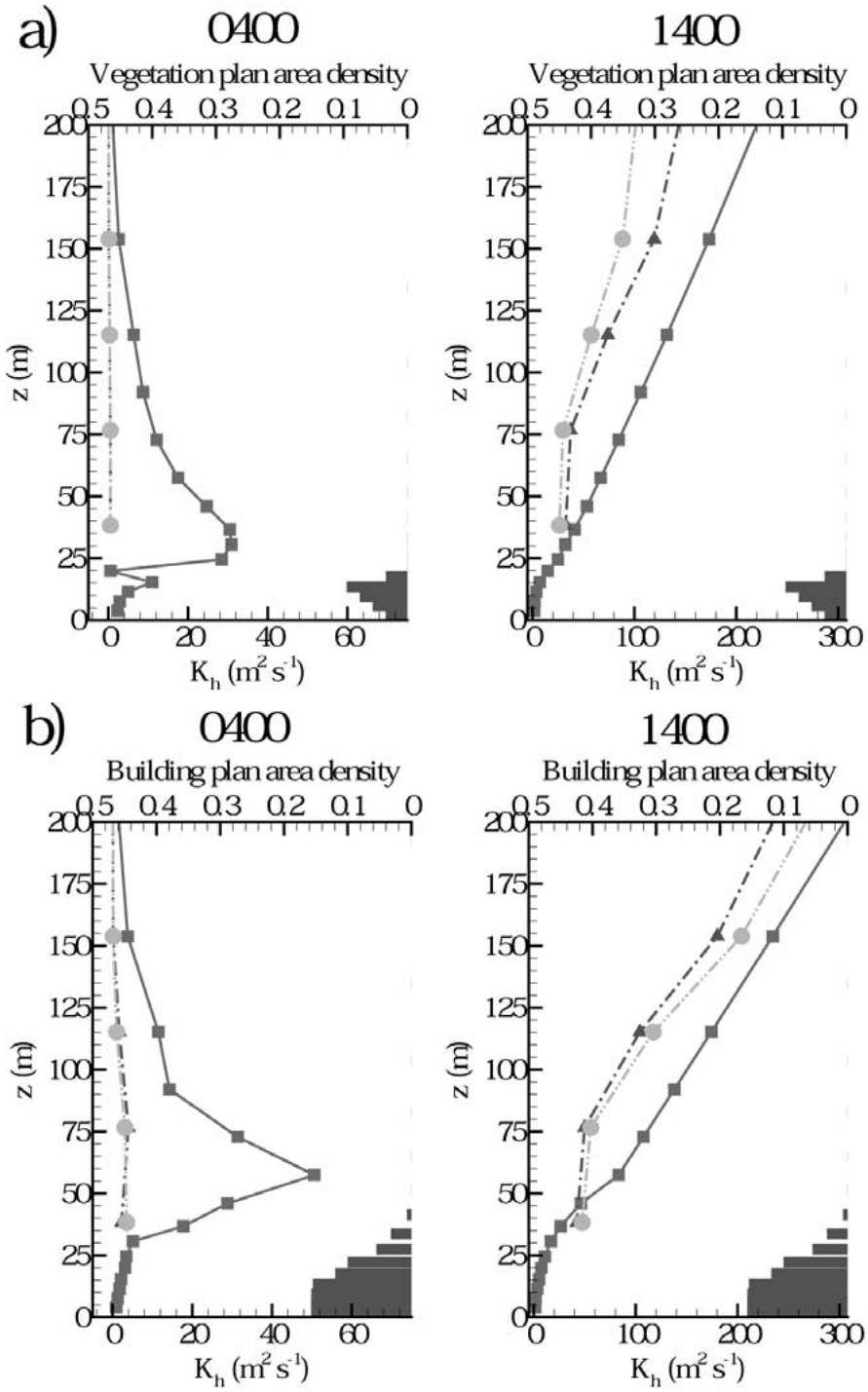

Figure 9. As in Figure 7, but for the eddy diffusivity.

canopy is observed because of the TKE maximum, whereas during the day, the discontinuity is non-existent contrary to the base simulation profile, which is not in agreement with observations, as discussed above. Thus, without changing the TLS parameterisation inside the canopy, the vertical diffusivity, i.e., the exchange, is increased between the inside and the outside of the canopy, which explains the smaller potential air temperature inside the canopy (see Figure 11) during the day.

By limiting the penetration of the large eddies inside the canopy (sim2), K_h is decreased within and above the canopy (Figure 10) with a smaller nocturnal peak above the canopies, and with a stronger discontinuity at the canopy-atmosphere interface during the day than for the based simulation, which induces also a stronger discontinuity on the potential air temperature profile (Figure 11). Thus, as expected, the exchange between the canopy and the upper atmosphere is reduced in sim2, increasing the potential air temperature by 0.5 to 0.6 K inside the canopy during the day. The nocturnal potential air temperature profiles from sim1 and sim2 are similar to DA-SM2-U (not shown).

Thus, the modification of the TLS parameterisation within the canopies in DA-SM2-U induces a discontinuity in the eddy diffusivity profile with smaller values inside the canopies, which seems to be consistent with previous observations (Denmead, 1964; Finnigan, 2000). We can thus expect to see a pollutant concentration discontinuity between the inside and the outside of the canopy. The nocturnal maximum of K_h above the canopies should increase the pollutant mixing in the upper part of the RSL, inducing a homogeneous layer. The limited sensitivity study of the TLS parameterisation presented in this section shows that this parameterisation is very delicate, and controls the intensity of the exchanges between the canopies and the atmosphere. This is supported by Finnigan (2000), who reported that K_h inside the canopy can become negative (countergradient diffusion) because of the non-local relationship between the flux and the gradient (e.g., the eddy diffusivity is not a useful description of the turbulent transport). Indeed, the vertical turbulent transport is not only influenced by the local vertical gradient but also by the non-local turbulent transport through the penetration of the large-scale eddies inside the canopy (Zeng and Takahashi, 2000). Thus, we can expect that the turbulent mixing should be under-estimated inside the canopy because of the limit of K-theory.

7. Surface Meteorological Fields and Energy Budgets

In this section, the air temperature and wind speed near the ground simulated by DA-SM2-U are compared with measurements from seven U.S. National Weather Service surface observation sites, including four in the urban area and three in the rural area, as represented in Figure 3a. The surface energy budgets and the vertical distribution of the heat fluxes within the canopies are also analysed so as to understand the behaviour of the new soil model SM2-U(3D).

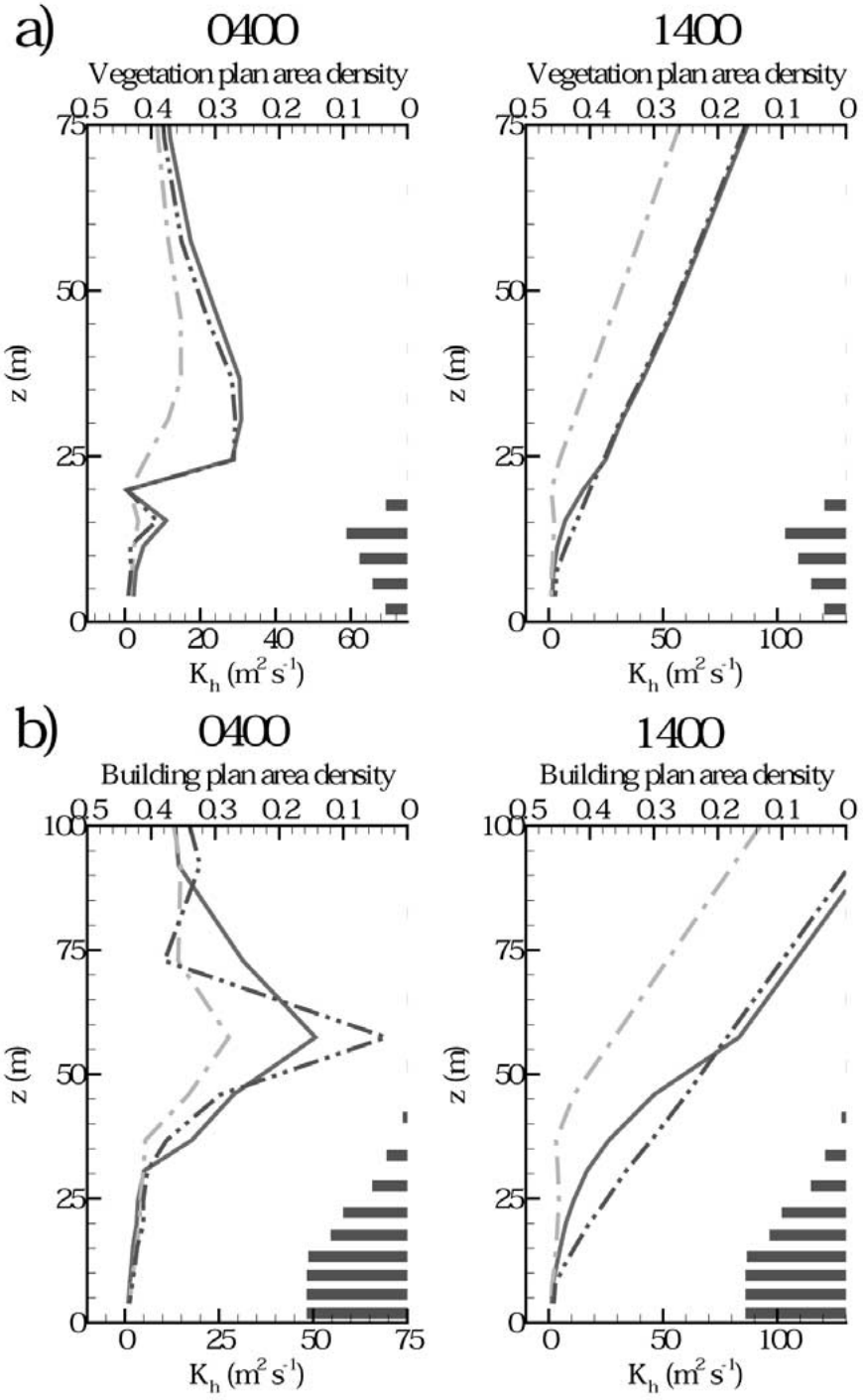

Figure 10. As in Figure 9, but for three different versions of DA-SM2-U: based case (solid line), sim1 (dashed dot dot line) and sim2 (dashed dot line).

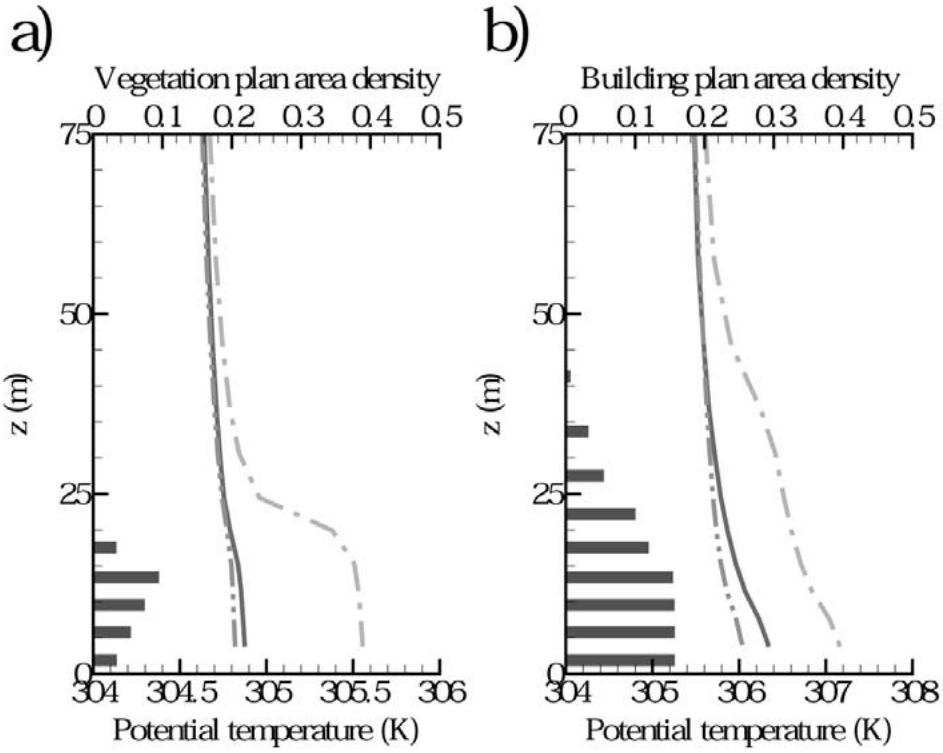

Figure 11. Vertical profiles of the potential air temperature for (a) a rural and (b) an urban point at 1400 local time, for three different versions of DA-SM2-U: base case (solid line), sim1 (dashed dot dot line) and sim2 (dashed dot line).

7.1. Comparison with observations

Figures 12 and 13 compare the 10-m wind speed and the 2-m air temperature (T_{air}) simulated by the three cases, RA-SLAB, RA-SM2-U and DA-SM2-U, with measurements averaged for the rural and urban stations. The air temperature and wind speed are reduced to observation height for the RA cases by extrapolation of values in the lowest computational layer by using the similarity theory, whereas they are directly simulated for DA-SM2-U.

The wind speed values simulated by the RA cases are very close together (Figure 12), and are higher than those simulated by DA-SM2-U. During the night, RA cases generally over-predict the wind speeds whereas the DA-SM2-U wind speeds match the observations slightly better. During the day, the wind speeds from the different cases are very close. The root mean square errors (RMSE) confirm these tendencies.

The 24-h evolution of T_{air} is generally well simulated by the three cases. For rural stations, during the night, the RA-SLAB case underestimates T_{air} (-2 °C), to a lesser extent for RA-SM2-U (-0.5 °C), whereas T_{air} is very close to observations

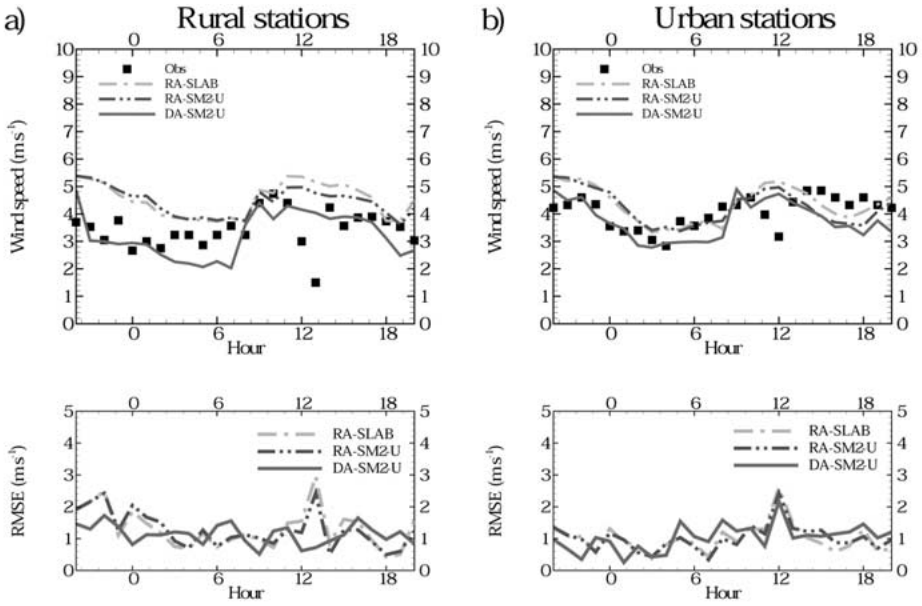

Figure 12. Comparison between the observed and simulated wind speeds at 10 m, averaged from (a) rural and (b) urban stations for the three MM5 versions. The root-mean square errors (RMSE = $[\sum_{i=1}^{n}(s_i - o_i)^2/n]^{1/2}$, with s_i and o_i, respectively the simulated and observed values, and $n = 3$ for rural stations and 4 for urban stations) are represented in the bottom figures.

for DA-SM2-U. During the day, T_{air} from DA-SM2-U is also very close to the observations, whereas RA cases slightly underestimates T_{air} in the evening. For urban stations, RA_SLAB underestimates (−2 °C) and overestimates (+2 °C) T_{air}, respectively, during the night and the day, whereas T_{air} from cases using SM2-U is very close to observations, except in the evening for DA-SM2-U where T_{air} is overestimated (+2 °C). The RMSE values confirm that the cases using SM2-U simulate T_{air} better than the RA-SLAB case, especially during the night for rural areas and during the full diurnal cycle for urban areas, except at the end of the day for DA-SM2-U.

Additional simulations based on the DA-SM2-U are performed to study the impact of the anthropogenic heat flux (Q_{urb}) and of the radiation extinction coefficient k_{ex} on the air temperature inside the canopy. Figure 14 shows, from the simulation with $Q_{\text{urb}} = 0$, that Q_{urb} only has an impact on T_{air} during the night and in the evening. During the day, mixing due to strong atmosphere instability is intense enough to disperse the heat emitted from anthropogenic sources throughout the PBL. These results are in agreement with the studies of Kimura and Takahashi (1991) and Khan and Simpson (2001). Without Q_{urb}, the nocturnal underestimation of T_{air} is increased, although the T_{air} overestimation in the evening simulated by the DA-SM2-U base simulation is attenuated. The evening T_{air} overestimation by the base simulation can possibly be due to a too large anthropogenic heat flux at that

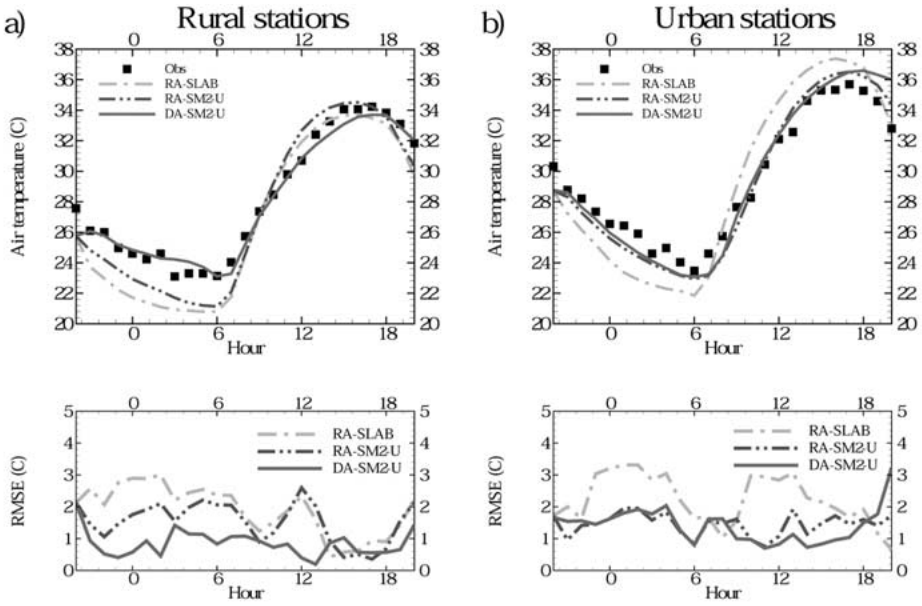

Figure 13. As in Figure 12, but for the air temperature at 2 m.

time of the day. The RA-SM2-U case, which uses the same Q_{urb} parameterisation as DA-SM2-U, does not overestimate T_{air} in the evening, but with the RA, Q_{urb} is emitted in the first layer of the computational domain whereas Q_{urb} is vertically distributed inside the urban canopy in the DA-SM2-U case. Thus, with the RA, Q_{urb} is more easily dispersed inside the PBL than with the DA where the canopy retains some of the heat, especially during the night.

As expected, k_{ex} only has an impact on T_{air} during the day (Figure 14). A zero value of k_{ex} (no shadowing effect) increases T_{air} inside the urban and rural canopies in comparison to the base simulation ($k_{\mathrm{ex}} = 1.5$), and inversely for $k_{\mathrm{ex}} = 3.0$. Neglecting the shadowing effect ($k_{\mathrm{ex}} = 0.0$) induces an overestimation of T_{air} during the day for the urban area and between 1000 and 1300 hours local time for the rural area, but it seems also to improve T_{air} for the rural area between 1300 and 1800 hours. It is difficult here to give definite conclusions on the correct value of k_{ex} because our choice of the vertical morphology of buildings and vegetation differs from the reality. However, between $k_{\mathrm{ex}} = 0.0$ and $k_{\mathrm{ex}} = 3.0$, the largest θ_{air} difference is only 1 K, but the thickness of the canopies where the surface observation stations are located, corresponds to just a few layers, especially for the urban stations.

7.2. Surface energy budgets

To understand the source of the differences between the ground air temperatures simulated by RA-SLAB, RA-SM2-U and DA-SM2-U, Figure 15 shows comparisons of average surface energy budgets above the rural and urban stations. For

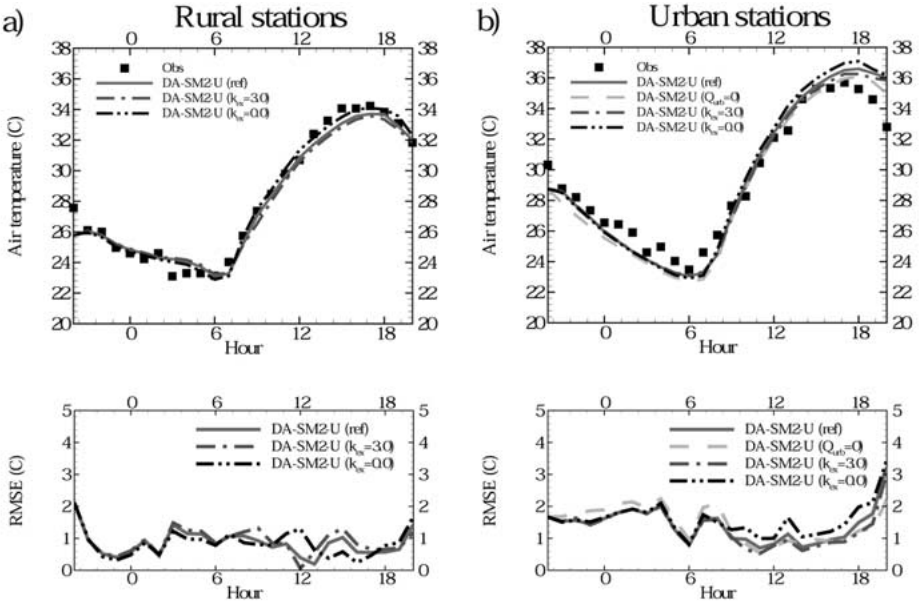

Figure 14. As in Figure 13, but for different sensitivities in DA-SM2-U.

DA-SM2-U, these average heat fluxes Φ_{tot} (where $\Phi \in \{R_n, H_{\text{sens}}, LE, G_s\}$) per unit of ground correspond to the vertical integration of the average heat fluxes emitted at each level inside the canopy:

$$\Phi_{\text{tot}} = \sum_j f_j \Phi_{\text{tot}j} \text{ for } j \in \{\text{bare, bui, nat, pav, vega, vegn, wat}\}, \tag{31}$$

with

$$\Phi_{\text{tot}j} = \sum_{k=0}^{k_{\text{top}}} \text{Surf}_j(k)\Phi_j(k) \text{ for } j \in \{\text{bare, bui, nat, vega, vegn, wat}\}, \tag{32}$$

and

$$\Phi_{\text{totpav}} = \sum_{k=0}^{k_{\text{top}}} \Phi^*_{\text{pav}}(k), \tag{33}$$

where f_j and Surf_j are defined in Section 2, Φ_j in Appendix A, and Φ^*_{pav} in Equation (27a, b).

Thus, keep in mind for the comparison that Φ_{tot} from DA-SM2-U can be assimilated to a heat flux at an 'energy displacement height', which corresponds to the average height of the exchange surfaces defined in Section 2, whereas Φ_{tot} from RA-SM2-U and RA-SLAB is a heat flux at the top of the canopy.

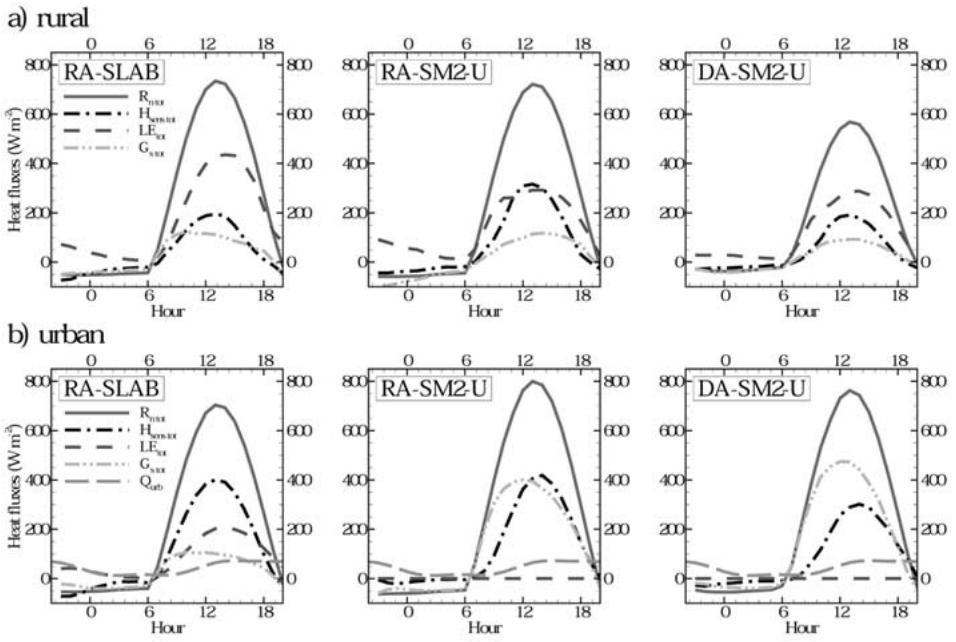

Figure 15. Surface energy budget averaged on (a) the rural and (b) urban stations, simulated by RA-SLAB, RA-SM2-U and DA-SM2-U.

The nocturnal rural energy budgets are characterized by a large latent heat flux (LE) for RA cases, which decreases during the night. The better nocturnal T_{air} simulated by DA-SM2-U seems to originate from a smaller LE. During the day, the storage heat fluxes (G_s) are very similar for the three cases. G_s seems slightly out of phase with the net radiation flux (R_n) for RA-SLAB. LE is the largest for RA-SLAB, and is always larger than the sensible heat flux (H_{sens}), except at midday for RA-SM2-U. The R_n maximum is smaller for DA-SM2-U than for the two other cases because of the shadowing effect; the R_n from RA-SLAB and RA-SM2-U is assessed at the top of the canopy.

For urban stations (Figure 15b), the anthropogenic heat flux (Q_{urb}) is identical for the three cases because the same parameterisation is used. The nocturnal warmer air simulated by RA-SM2-U and DA-SM2-U compared to RA-SLAB (Figure 13b) can be explained by a smaller LE (zero for RA-SM2-U and negative for DA-SM2-U). During the day, the energy budgets simulated by the cases using SM2-U are very different from RA-SLAB. In the SM2-U model, the urban surfaces are complex, whereas in the SLAB soil model they are represented by a dry bare soil. For RA-SLAB, the differences between the rural and urban energy budgets arise only from the decrease of LE in urban areas, inducing an increase of H_{sens}, G_s remaining similar. The LE maximum in urban areas simulated by RA-SLAB is around 200 W m^{-2} whereas it is zero for RA-SM2-U and DA-SM2-U. This zero value of LE is due to the rough representation of the vegetation in the USGS

classification for dense urban areas. Thus, most of the urban areas are considered without natural surfaces, which is certainly erroneous. We can expect that LE is underestimated by RA-SM2-U and DA-SM2-U but the LE from RA-SLAB seems too large. With SM2-U, G_s is larger than H_{sens} and LE during the day, which has been observed in a few dense urban areas (c.f. Grimmond and Oke, 1999) because of the radiative trapping and of the heat storage by roofs, walls, and paved surfaces. Conversely, for RA-SLAB, G_s is lower than H_{sens} and LE. The overestimation of T_{air} by RA-SLAB in the morning is due to the underestimation of G_s and to the overestimation of H_{sens}, as urban surfaces generally store energy after sunrise before warming up, as simulated by SM2-U. G_s is slightly lower and H_{sens} higher with RA-SM2-U than with DA-SM2-U. In the evening, H_{sens} is higher than G_s for DA-SM2-U, whereas G_s is close to H_{sens} for RA-SM2-U, which explains a part of the higher T_{air} simulated by DA-SM2-U. As seen above, a large part of the overprediction of the evening urban T_{air} is explained by a too large anthropogenic heat flux, which is maximized in the evening. The parameterisation of Q_{urb} should be probably reviewed, especially its time variation. This overprediction can be also attributed to the crude representation of the urban morphology and to the underestimation of the vegetation in urban areas although the extrapolated T_{air} of the RA-SM2-U case seems well simulated.

7.3. Vertical distribution of heat fluxes within the canopy

The vertical distribution of the heat fluxes inside the canopies simulated by the DA-SM2-U base case ($k_{\text{ex}} = 1.5$) is represented in Figures 16a and 17a at 0400, 1400 and 2000 local time, respectively for the rural and urban points defined in Figure 3a. These points have been preferred to the surface observation stations because the vegetation and building canopies are thicker, which facilitates the understanding of the model behaviour. However, the surface energy budgets at these points (not shown) have the same characteristics as those presented in Figure 15. During the night (0400 local time), evaporation is produced by the lower part of the vegetation foliage whereas condensation is produced at the top of the vegetation canopy, which is cooler; this can explain the lower LE simulated by DA-SM2-U than by RA- SM2-U. For the urban canopy, the anthropogenic heat fluxes are larger in the lower part of the canopy because they are vertically distributed following the plan area density of the buildings (Equation (B9)). The roofs of the higher buildings are colder than those of the smaller buildings, which induces a larger negative value of H_{sens} at the top of the canopy. Deeper inside the canopy, H_{sens} becomes positive because of the large release of energy that has been stored during the day by roofs and walls. The stronger roof cooling at the top of the canopy can be explained by the larger heat exchange at this level induced by the larger wind speed and larger TKE. This large heat exchange, characterized by a large magnitude of H_{sens}, is observed throughout the day. Thus, the maximum magnitudes of H_{sens} and R_n occur at the top of the canopy whereas the maximum of G_s occurs at 2/3 of the

height of the canopy. H_{sens} decreases inside the canopy and approaches zero in the lower part of the canopy because of the shadowing effects. In the evening (2000 local time), the upper part of the canopy starts to release heat before the lower part.

The Figures 16b and 17b are the same as Figures 16a to 17a but for $k_{ex} = 0.0$ and $k_{ex} = 3.0$. As expected, the increase of k_{ex} decreases R_n inside the canopies, which decreases also the other fluxes and the air temperature. Without radiative extinction ($k_{ex} = 0.0$), the nocturnal condensation occurs throughout the depth of the vegetation foliage whereas with k_{ex} larger than 1.5, it occurs only on the upper part, as evaporation occurs in the lower part. For k_{ex} larger than 1.5, the nocturnal H_{sens} is positive in the lower part of the urban canopy and negative in the upper part whereas it is always negative or zero for $k_{ex} = 0.0$.

8. Meteorological Fields within and above the Canopies

The air temperature and the wind fields near the ground are particularly dependent on the structure of the urban and rural canopies and on their parameterisation, as well as on the heat fluxes emitted by the canopy elements. Just above the canopy, these meteorological fields are influenced by the heat and momentum fluxes from the canopies. Their correct simulation is critical since it is principally at this level that the pollutants arising from the canopy are dispersed toward neighbouring areas. In this section, the potential air temperature and wind fields simulated by DA-SM2-U are analysed in a horizontal cross-section of the computational domain within the canopy, and are compared with the fields simulated by RA-SM2-U and RA-SLAB in a horizontal cross-section situated just above the canopy.

8.1. Within the canopy

Figure 3b represents the principal land-use categories: water, urban, vegetation canopy and open areas. The vegetation canopy category corresponds to the vegetation higher than the middle of the first layer, and the open area category indicates no canopy (i.e., small vegetation and/or bare soil). To analyse the behaviour of the wind and air temperature fields within the canopies simulated by DA-SM2-U, we focus on a part of the computational domain that includes both vegetation canopies and urban canopies (see Figure 18a). Figures 18b, c and d represent the wind and potential air temperature fields inside this smaller domain at 2 m above the ground, respectively at 0400, 1400 and 2000 local time. These figures show the decrease of the wind speed inside the rural and urban canopies, and the skirting of the flow around the vegetation canopy blocks, especially during the night (0400 local time) and for the tree block located around the coordinates (63, 20). From the potential air temperature field, it is also possible to distinguish the rural and urban canopies from the open areas. The nocturnal potential air temperature is higher inside the vegetation canopies than above open areas because of the small ventilation inside

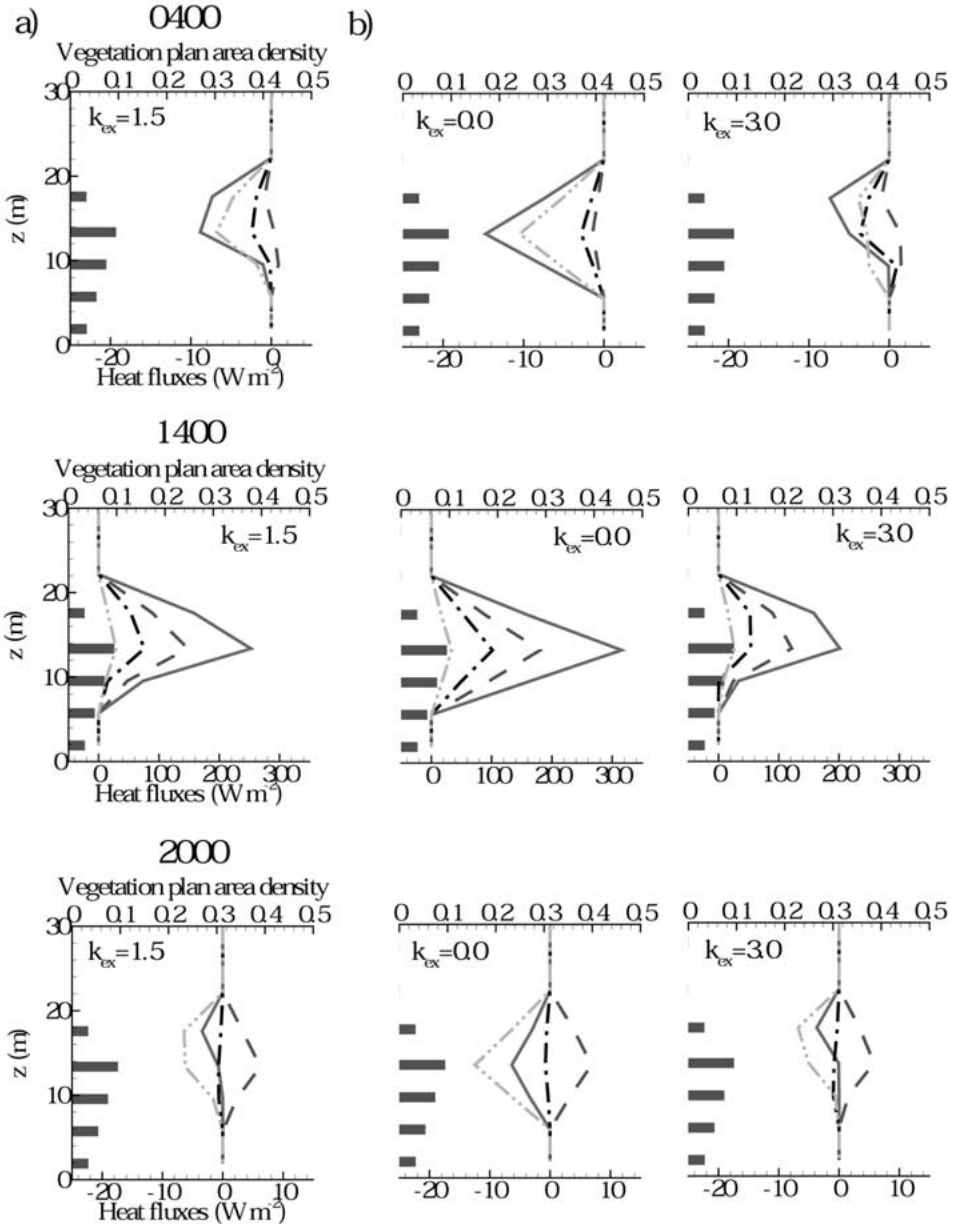

Figure 16. Vertical profiles of the heat fluxes simulated by DA-SM2-U for a rural point at 0400, 1400 and 2000 local time, for (a) the base simulation and for (b) two other simulations with different values of the radiative extinction coefficient k_{ex}. Net radiation flux (solid line), sensible heat flux (dashed dot line), latent heat flux (dashed line) and storage heat flux (dashed dot dot line).

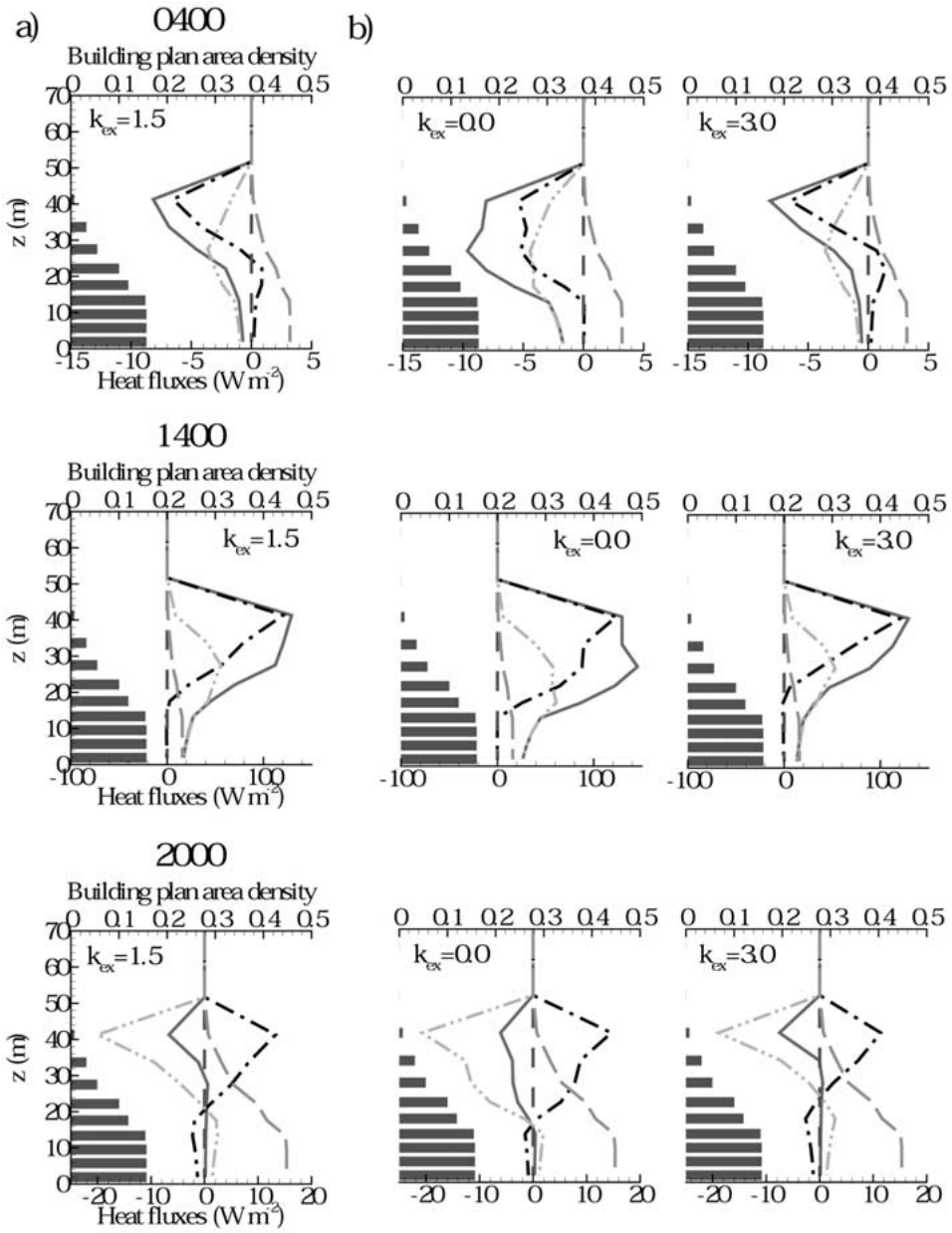

Figure 17. As in Figure 16, but for an urban point. Anthropogenic heat flux (long dashed line).

the canopies that reduces the decrease of the temperature. The air inside the urban canopy is slightly warmer than within the vegetation canopy, especially downtown because of the heat released by the urban artificial surfaces and by the anthropogenic sources. Conversely during the day, the air within the vegetation canopies is colder than above open areas because of the shadowing effect, and of the large latent heat flux emitted by the vegetation. The urban canopy is the warmest area because of the anthropogenic heat flux emissions, of the large sensible heat flux from the artificial surfaces and of the very small latent heat flux. Additionally, the small ventilation inside the rural and urban canopies accentuates the difference of temperature between the air inside the canopies and above the open areas by decreasing the renewal of air. At the end of the day, the air temperature decreases rapidly above the open areas whereas the air remains warm within the canopies, as observed during the night. A large urban heat island can be observed with a convergence of the flow toward the city.

8.2. ABOVE THE CANOPY

Figure 19 represents the wind and potential air temperature fields at 55 m above the ground for the full domain, which is generally situated above the canopies, simulated by the three cases at 0400, 1400 and 2000 local time. Throughout the day, the wind direction is generally south-westerly. The nocturnal air is warmer for RA-SLAB and RA-SM2-U above and downwind of the city, whereas it is warmer on the north-west side of the city for DA-SM2-U. The DA-SM2-U colder air above the city can be explained by the presence of a corridor on the east side of the city between downtown and the east vegetation canopies (see Figure 18a), which is not represented in the RA. This corridor, composed of open areas, induces a stronger wind speed than with the RA cases, advecting colder air from rural areas to the city, and also slightly advecting the warmer air produced by the city towards the north-west side of the city. Warmer air is also observed above the higher vegetation canopies. It seems to be explained more by the increase of the mixing just above the canopy than by the exchange between the warmer air within the canopy and the air above. Indeed, the additional simulation, sim2 (presented in the Subsection 6.6.) where the penetration of the large eddies is reduced inside the canopy by limiting l_{up} and l_{down}, does not change the nocturnal air temperature above the canopy (not shown). The larger mixing simulated by DA-SM2-U above the vegetation canopy, induced by the TKE maximum, can be seen in the potential air temperature profile (Figure 7a). The potential air temperature is larger between 25 and 70 m with DA-SM2-U than with RA cases, and conversely between 70 and 200 m. During the day (1400 local time), an urban heat island is simulated by RA-SLAB with an amplitude of 3–4 K, and to a lesser extent for RA-SM2-U and DA-SM2-U with an amplitude of 1 K. The presence of a small heat island during the day, as simulated by SM2-U cases, is in agreement with previous observations over many cities (Oke, 1978), which is also confirmed by the overestimation of the surface air

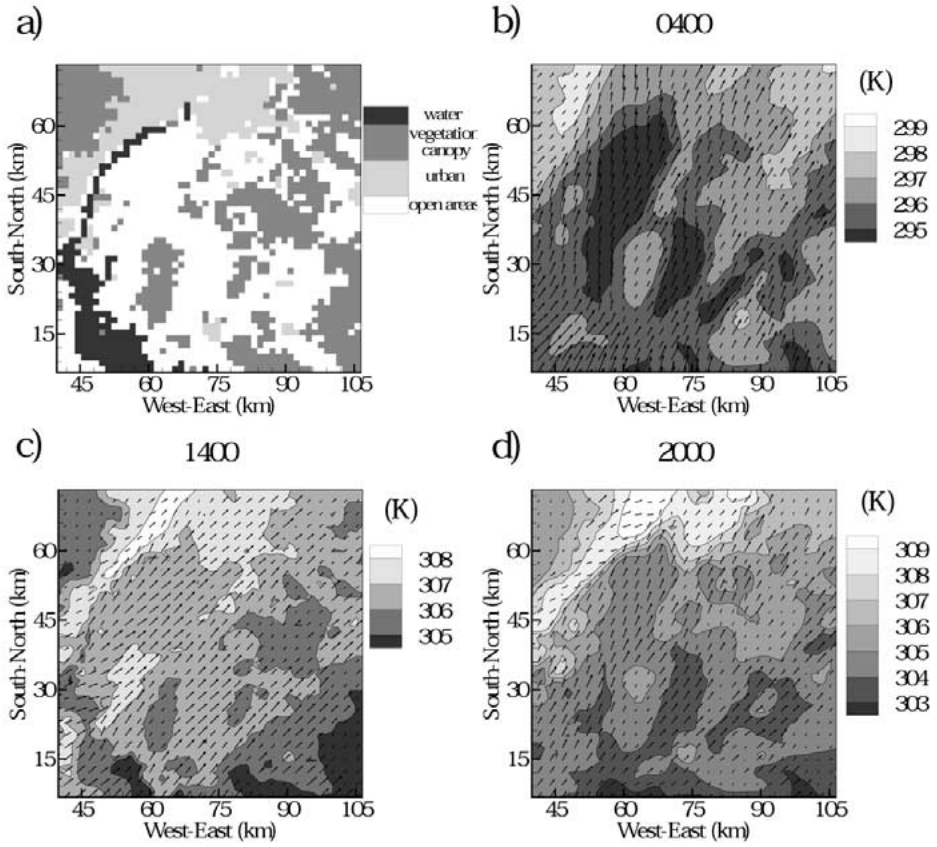

Figure 18. Wind vector and potential air temperature fields simulated by DA-SM2-U, at 0400 (b), 1400 (c) and 2000 (d) local time, at 2 m above the ground in a part of the computational domain represented in (a), which is a zoom of Figure 3a.

temperature by RA-SLAB, seen in Subsection 7.1. In the evening, a strong heat island is simulated by the three cases ($\approx$ 5 to 6 K). The north-west side of the domain is slightly warmer for DA-SM2-U than for the other cases, for the same reasons as during the night. This concentration of heat over the city induces a flow convergence over the urban area that is stronger for DA-SM2-U.

Because of the lack of measurements, and of the rough representation of the vegetation and building canopies, this analysis of meteorological fields simulated by DA-SM2-U within and above the canopies does not allow us to make a judgment about the accuracy of the simulation against the reality within the canopies, and on their improvement or not with the DA against the RA. However, the modifications simulated by DA-SM2-U on the air temperature and wind fields seem to be consistent with the canopy morphology used here. The larger nocturnal mixing above the

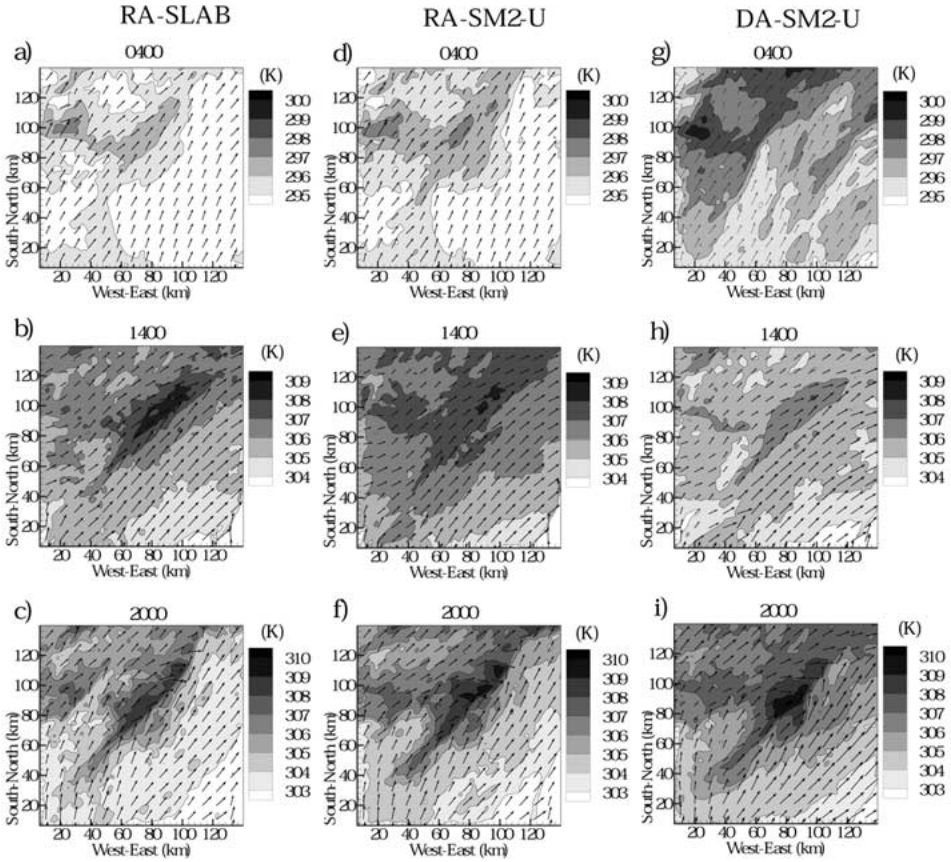

Figure 19. Wind vector and air potential temperature fields at 50 m above the ground for the full domain, simulated by the three MM5 versions: RA-SLAB (a, b and c), RA-SM2-U (d, e and f) and DA-SM2-U (g, h and i), at 0400, 1400 and 2000 local time.

vegetation canopies inducing warmer air may be too large, and which may result from a deficiency in the turbulent scheme model.

9. Summary

One of the key aspects for air quality predictions to assess human exposure and human risk at neighbourhood scales (on order of 1-km horizontal grid spacing) is the accurate simulation of the meteorological fields inside the roughness sub-layer (RSL). Since the assumptions of the roughness approach (RA) are unsatisfactory at this scale, a detailed urban and rural canopy parameterisation, called DA-SM2-U, has been developed inside MM5 to simulate the meteorological fields within and above the urban and rural canopies. DA-SM2-U uses the drag-force approach (DA)

to represent the dynamic and turbulent effects of the buildings and vegetation, and a modified version of the soil model SM2-U, called SM2-U(3D), to represent the thermodynamic effects of the canopy elements. SM2-U(3D) is capable of assessing the heat fluxes from rural and urban surfaces in each computational layer inside the canopies.

DA-SM2-U has been tested in a real case above Philadelphia, in Pennsylvania, U.S.A., during one summer day, and compared with two other simulations using the RA: the first one corresponds to the standard version of MM5 (RA-SLAB) and the second one is coupled with SM2-U (RA-SM2-U). The analysis of the dynamic, turbulent, and thermodynamic vertical profiles inside the urban and rural RSL has shown a realistic behaviour of DA-SM2-U, consistent with observed data in urban and vegetation canopies and simulated data in wind-tunnel studies. The shear stress is characterized by a maximum near the top of the canopy, followed by a decrease inside the canopy. The general features of the vertical components of the turbulent kinetic energy (TKE) within and above the vegetation canopy agree very well with simulations and observations reported in the literature. A discontinuity in the eddy diffusivity profile is simulated by DA-SM2-U between the canopies and the upper atmosphere, with small values of the eddy diffusivity inside the canopies, inducing a limitation of the turbulent exchanges between the inside and the outside of the canopies. This discontinuity is due to the modification of the turbulent length scale (TLS) parameterisation inside the canopies. We can thus expect to find this discontinuity on the simulated pollutant fields. During the night, the eddy diffusivity maximum is simulated just above the canopies, which increases the mixing in the upper part of the RSL. This maximum is not simulated with the RA. However, this increase of the turbulent mixing induced by the TKE maximum seems too large above the vegetation, inducing a too high neutral layer. The vertical profiles of the potential air temperature in urban areas have shown that simulations using SM2-U reduce the tendency toward stable stratification. They even yield a neutral layer during the night because of the anthropogenic heat fluxes and also the heat released by urban surfaces.

Within the canopies, the DA-SM2-U meteorological fields seem well simulated following the canopy morphology: decrease of the wind speed inside the dense canopies, skirting of the flow around the canopy blocks, warmer air inside the vegetation canopy than above open areas during the night and conversely during the day, and constantly warmer air inside the urban canopy. By comparison with measurements, the surface air temperatures simulated with SM2-U have been improved throughout the day for rural and urban stations, especially with the DA for rural stations. However, DA-SM2-U overestimates the air temperature in the evening inside the urban canopy, a large part of this overestimation being due to the anthropogenic heat fluxes, which are probably too large at this time of the day. This was not observed with the RA because the anthropogenic heat fluxes are emitted in the first layer, which included the entire RSL, and thus heat is more

easily dispersed inside the PBL than with the DA where the canopy retains much of the heat.

From a limited sensitivity study, the results indicate a sensitivity to the TLS parameterisation inside the canopies, which means that the processes of momentum and heat exchanges between the canopy and the atmosphere need to be better understood, especially in urban areas, to improve the TLS parameterisation or the turbulent scheme inside the RSL. Furthermore, the use of a local closure turbulence scheme in the canopy is probably questionable since the vertical turbulent transport is not only influenced by the local vertical gradient but also by the non-local turbulent transport through the penetration of the large-scale eddies inside the canopy (Zeng and Takahashi, 2000).

Finally, the improvement of the rural and urban canopies representation in mesoscale models requires additional input data characterizing the canopies. For this Philadelphia study, we used a rough representation of the vegetation and building canopies, which could certainly have an impact on the realism of the simulated meteorological fields in certain parts of the computational domain. The urban morphological data are becoming accessible for many cities but remain expensive. For future studies, the sensitivity of the degree of detail of the canopy morphological data on the meteorological fields needs to be assessed.

Acknowledgements

The first author was supported at the Atmospheric Sciences Modeling Division through UCAR Visiting Scientist Program appointments. The second and third authors were supported by EPA Interagency Agreement DW13938634 with NOAA.

Appendix A: Vertical Turbulent Transport Parameterization

As proposed by Martilli et al. (2002), the effects of the volume occupied by buildings on the turbulent vertical fluxes are considered by neglecting them inside buildings. The volume of the vegetation is neglected.

Thus,

$$\frac{\partial \langle w\phi \rangle}{\partial z} = \frac{1}{V_{\text{air}}}[\langle w\phi \rangle(k) - \langle w\phi \rangle(k+1)], \tag{A1}$$

with $\phi \in \{u_x, u_y, q_w, E, \theta_L\}$.

The vertical turbulent momentum flux is:

$$\langle w\phi \rangle = -K_m \frac{\partial \langle \phi \rangle}{\partial z} S_{\text{air}}, \tag{A2}$$

with $\phi \in \{u_x, u_y\}$.

The vertical turbulent humidity flux is

$$\langle w q_w \rangle = -K_h \frac{\partial \langle q_w \rangle}{\partial z} S_{\text{air}}, \tag{A3}$$

and the vertical turbulent heat flux is

$$\langle w \theta_L \rangle = -K_h \left[\frac{\partial \langle \theta_L \rangle}{\partial z} - \gamma_g \right] S_{\text{air}}, \tag{A4}$$

where γ_g is the countergradient term (Therry and Lacarrère, 1983), and K_m and K_h are respectively the momentum and heat eddy diffusivities.

Note, that in the turbulent vertical heat flux, the parameterisation of the countergradient term used by the GSPBL model, which was based in Musson-Genon (1987), has been modified:

$$\gamma_g(k) = \begin{cases} \left(\dfrac{5}{w_* h}\right)\left(\dfrac{1}{\rho(k) c_p}\right) H_{\text{sens cum}}(k) & z < 1.2h \\ 0 & z \geq 1.2h \end{cases}, \tag{A5}$$

with

$$H_{\text{sens cum}}(k) = \sum_{p=0}^{k} H_{\text{sens mean}}(p), \tag{A6}$$

where h is the height of the convective layer and $H_{\text{sens cum}}$ the total sensible heat flux emitted between the ground and the level k.

At the ground surface

$$\langle w u_x \rangle_{\text{surf}} = -\frac{[u_{*\text{mean}}(0)]^2 \langle u_x(k=1) \rangle}{\sqrt{\langle u_x(k=1) \rangle^2 + \langle u_y(k=1) \rangle^2}} \text{Surf}_{\text{tot}}(0), \tag{A7}$$

$$\langle w \theta_L \rangle_{\text{surf}} = \frac{H_{\text{sens mean}}(0)}{\rho(1) c_p}, \tag{A8}$$

$$\langle w q_w \rangle_{\text{surf}} = \frac{E_{\text{mean}}(0)}{\rho(1)}. \tag{A9}$$

The eddy diffusivities are assessed from,

$$K_\Phi = L_\Phi \sqrt{E}, \tag{A10}$$

where $\Phi \in \{h, m\}$.

L_Φ, which depends on the TLS, l, is determined from Ballard et al. (1991), except during unstable conditions where

$$L_\phi = 0.40l\sqrt{E}. \tag{A11}$$

Appendix B: Surface Temperatures and Heat Fluxes assessed by SM2-U(3D)

Surface temperatures

The temperature $T_{sj}(k)$ of the surface type 'j' at the level k is evaluated from a force-restore equation, except for roofs where their temperatures are determined by a simple heat conduction equation in a solid. The determination of the water surface temperature depends on its type. Thus,

$$\frac{\partial T_{sj}(k)}{\partial t} = C_{Tj}(k)G_{sj}(k) - \frac{2\pi}{\tau}[T_{sj}(k) - T_{\text{soil}}], \tag{B1}$$

for $j \in \{\text{bare, nat, pav, vega, vegn}\}$,

$$\frac{\partial T_{s\text{bui}}(k)}{\partial t} = C_{T\text{bui}}(k)G_{s\text{bui}}(k), \tag{B2}$$

where $k \in [0, k_{\text{top}}]$, $C_{Tj}(k)$ represents the surface resistance to the atmospheric forcing at the level k, T_{soil} is the soil temperature, and $\tau = 86{,}400$ s.

C_{Tj} and T_{soil} are parameterised in the same way as in SM2-U (Dupont, 2001). Note that in SM2-U, $C_{T\,\text{pav}}$ is represented as two resistances in parallel: one for the walls and the other one for the paved surfaces.

The stored heat flux $G_{sj}(k)$ is obtained by closing the energy budget of the surface:

$$G_{sj}(k) = R_{nj}(k) - LE_j(k) - H_{\text{sens}j}(k) - \delta_{j\text{pav}}\left(\frac{2z(k)}{W(k)}\right)Q_{\text{wall}}, \tag{B3}$$

where R_{nj} is the net radiation flux (Equation (24)), E the water vapour flux (Equations (B5) and (B8)), H_{sens} the sensible heat flux (Equation (B4)), Q_{wall} the building heat flux (Equation (B11)), and δ is the Kronecker's symbol ($\delta_{\text{pav pav}} = 1$ and $\delta_{j\,\text{pav}} = 0$ for $j \neq \text{pav}$).

Heat fluxes

The SM2-U parameterisations of the sensible heat and water vapour fluxes are extended here to all levels inside the canopy. Thus, the flux at the level k depends on the variables at the level k and $k + 1$.

• Sensible heat flux

$$H_{\text{sens}j}(k) = \rho(k+1)c_p \frac{1}{R_{ahj}(k)}[\theta_{sj}(k) - \theta(k+1)], \tag{B4}$$

where R_{ah} is the aerodynamic heat resistance, and θ_s the potential surface temperature.

• Water vapour flux

The water vapour flux from the vegetation, E_j, is the sum of the evaporation of the intercepted water by the vegetation, E_{rj}, and of the vegetation transpiration, E_{trj}:

$$E_j(k) = E_{rj}(k) + E_{trj}(k) \tag{B5}$$

with

$$E_{rj}(k) = \frac{\rho(k+1)\delta_j(k)}{R_{aqj}(k)}[q_{v\,\text{sat}j}(k) - q_v(k+1)], \tag{B6}$$

$$E_{trj}(k) = \frac{\rho(k+1)\lfloor 1 - \delta_j(k)\rfloor}{R_{aqj}(k) + R_{sj}(k)}[q_{v\,\text{sat}j}(k) - q_v(k+1)], \tag{B7}$$

where $k \in [0, k_{\text{top}}]$, $j \in \{\text{vega}, \text{vegn}\}$, δ_j is vegetation surface wet portion, R_{aq} and R_s the aerodynamic humidity and stomatal resistances, and $q_{v\,\text{sat}}$ the surface saturated specific humidity of the air.

The water vapour fluxes from artificial surfaces are determined in the same way as the evaporation fluxes from the vegetation, by extending the concept of the vegetation surface wet portion to urban surfaces:

$$E_j(k) = \frac{\rho(k+1)\delta_j(k)}{R_{aqj}(k)}[q_{v\,\text{sat}j}(k) - q_v(k+1)], \tag{B8}$$

where $k \in [0, k_{\text{top}}]$, $j \in \{\text{bui}, \text{pav}\}$, and δ_j is the artificial surface wet portion.

The parameterisations of δ, R_s and $q_{v\,\text{sat}}$ are identical as in SM2-U but extended to the level k.

The aerodynamic humidity and heat resistances, which appear in the parameterisation of the sensible heat and water vapour transfers, are deduced from Guilloteau (1998). They are determined for each surface type and at each level inside the canopy following the local characteristics of the atmosphere and of the considered surface. The conditions of validity of the similarity theory is questionable at this scale but we do not know a better parameterisation.

• Anthropogenic heat flux

The anthropogenic heat flux, Q_{urb}, is parameterised following Lacser and Otte (2002) where its temporal variation is defined following Taha (1999). It is distributed inside the canopy following the vertical distribution of buildings:

$$Q_{\mathrm{urb}}(k) = Q_{A\,\max} \frac{A_{p\mathrm{bui}}(k)}{\sum_{p=1}^{k_{\mathrm{top}}} A_{p\mathrm{bui}}(p)} F(t), \tag{B9}$$

with

$$F(t) = \gamma + \sum_{n=1}^{3} \left[\lambda_n \cos\left(\frac{2n\pi t}{24}\right) + \phi_n \sin\left(\frac{2n\pi t}{24}\right) \right], \tag{B10}$$

where $Q_{A\,\max}$ is the maximum anthropogenic heat flux, which is modulated diurnally by the Fourier series, $F(t)$, for t in hours. For Philadelphia, $Q_{A\,\max} = 50$ W m^{-2} for residential areas and $Q_{A\,\max} = 100$ W m^{-2} for dense and industrial urban areas.

Following Taha (1999), $\gamma = 0.557$, $\lambda_1 = -0.227$, $\lambda_2 = -0.006$, $\lambda_3 = -0.084$, $\Phi_1 = -0.384$, $\Phi_2 = 0.016$, and $\Phi_3 = -0.012$. This series represents the summertime anthropogenic heating profile deduced from energy studies of various cities.

• Building heat flux

The heat flux through building walls depends on the wall heat transfer coefficient K_{wall} and on the temperature difference between the outside and the inside of buildings:

$$Q_{\mathrm{wall}}(k) = K_{\mathrm{wall}}(T_{s\,\mathrm{pav}}(k) - T_{\mathrm{int}}), \tag{B11}$$

where $T_{s\,\mathrm{pav}}$ is the mean temperature of the surfaces of the street and T_{int} is the air temperature inside the buildings, fixed at 291 K. Following Dupont (2001), $K_{\mathrm{wall}} = 1.3$ W m^{-2} K^{-1}.

References

Ballard, S. P., Golding, B. W., and Smith, R. N. B.: 1991, 'Mesoscale Model Experimental Forecasts of the Haar of Northeast Scotland', *Mon. Wea. Rev.* **119**, 2107–2123.

Bélair, S., Lacarrère, P., Noilhan, J., Masson, V., and Stein, J.: 1998, 'High-Resolution Simulation of Surface and Turbulent Fluxes during HAPEX-MOBILHY' *Mon. Wea. Rev.* **126**, 2234–2253.

Bélair, S., Mailhot, J., Strapp, J. W., and MacPherson, J. I.: 1999, 'An Examination of Local versus Nonlocal Aspects of a TKE-Based Boundary Layer Scheme in Clear Convective Conditions', *J. Appl. Meteorol.* **38**, 1499–1518.

Bougeault, P. and Lacarrère, P.: 1989, 'Parameterization of Orography-Induced Turbulence in a Mesobeta-Scale Model', *Mon. Wea. Rev.* **117**, 1872–1890.

Brown, M. J: 2000, 'Urban Parameterizations for Mesoscale Meteorological Models', in Z. Boybeyi (ed.), *Mesoscale Atmospheric Dispersion*, Wessex Press, 448 pp.

Brunet, Y., Finnigan, J. J., and Raupach, M. R.: 1994, 'A Wind Tunnel Study of Air Flow in Waving Wheat: Single-Point Velocity Statistics', *Boundary-Layer Meteorol.* **70**, 95–132.

Ca, V. T., Ashie, Y., and Asaeda, T.: 2002, 'A $k - \varepsilon$ Turbulence Closure Model for the Atmospheric Boundary Layer Including Urban Canopy', *Boundary-Layer Meteorol.* **102**, 459–490.

Denmead, O. T.: 1964, 'Evaporation Sources and Apparent Diffusivities in a Forest Canopy', *J. Appl. Meteorol.* **3**, 383–389.

Dupont, S.: 2001, *Modélisation dynamique et thermodynamique de la canopée urbaine: réalisation du modèle de sols urbains pour SUBMESO*, Doctoral thesis, Université de Nantes, France.

Dupont, S., Calmet, I., and Mestayer, P. G.: 2002, 'Urban Canopy Modeling Influence on Urban Boundary Layer Simulation', in *AMS 4th Symposium on Urban Environment*, Norfolk, Virginia, 20–24 May 2002, Proceedings, pp. 151–152.

Ellefsen, R.: 1990–1991, 'Mapping and Measuring Buildings in the Canopy Boundary Layer in Ten U.S. Cities', *Energ. Buildings* **15–16**, 1025–1049.

Finnigan, J. J.: 2000, 'Turbulence in Plant Canopies', *Annu. Rev. Fluid. Mech.* **32**, 519–571.

Green, S. R.: 1992, 'Modelling Turbulent Air Flow in a Stand of Widely-Spaced Trees', *PHOENICS J. Comp. Fluid. Dyn. Appl.* **5**, 294–312.

Grell, G., Dudhia, J., and Stauffer, D. R.: 1994, *A Description of the Fifth-Generation Penn State/NCAR Mesoscale Model (MM5)*, NCAR/TN-398+STR, 138 pp.

Grimmond, C. S. B. and Oke, T. R.: 1999, 'Heat Storage in Urban Areas: Local-Scale Observations and Evaluation of a Simple Model', *J. Appl. Meteorol.* **38**, 922–940.

Guilloteau, E.: 1998, 'Optimized Computation of Transfer Coefficients in Surface Layer with Different Momentum and Heat Roughness Lengths', *Boundary-Layer Meteorol.* **87**, 147–160.

Hamlyn, G. J.: 1992, *Plants and Microclimates, a Quantitative Approach to Environmental Plant Physiology*, Cambridge University Press, U.K., 428 pp.

Inclan, M. G., Forkel, R., Dlugi, R., and Stull, R. B.: 1996, 'Application of Transilient Turbulent Theory to Study Interactions between the Atmospheric Boundary Layer and Forest Canopies', *Boundary-Layer Meteorol.* **79**, 315–344.

Kaimal, J. C. and Finnigan, J. J.: 1994, *Atmospheric Boundary Layer Flows. Their Structure and Measurements*, Oxford University Press, New York, 289 pp.

Kanda, M. and Hino, M.: 1994, 'Organized Structures in Developing Turbulent Flow within and above a Plant Canopy, Using a Large Eddy Simulation', *Boundary-Layer Meteorol.* **68**, 237–257.

Kastner-Klein, P.: 2001, 'Overview of Near-Surface Turbulence Parameterizations', in *Preprint COST 715 Workshop on Urban Boundary Layer Parameterizations*, Zurich, May 24/25.

Khan, S. M. and Simpson, R. W.: 2001, 'Effect of a Heat Island on the Meteorology of a Complex Urban Airshed', *Boundary-Layer Meteorol.* **100**, 487–506.

Kimura, F. and Takahashi, S.: 1991, 'The Effects of Land-Use and Anthropogenic Heating on the Surface Temperature in the Tokyo Metropolitan Area: A Numerical Experiment', *Atmos. Environ.* **25B**, 155–164.

Lacser, A. and Otte, T. L.: 2002, 'Implementation of an Urban Canopy Parameterization in MM5', Preprints, in *Fourth Symposium on Urban Environment*, American Meteorological Society, Norfolk, VA, pp. 153–154.

Leclerc, M. Y., Beissner, K. C., Shaw, R. H., Hartog, G. D., and Neumann, H. H.: 1990, 'The Influence of Atmospheric Stability on the Budgets of the Reynolds Stress and Turbulent Kinetic Energy within and above a Deciduous Forest', *J. Appl. Meteorol.* **29**, 916–933.

Liu, J., Chen, J. M., Black, T. A., and Novak, M. D.: 1996, '$k - \varepsilon$ Modelling of Turbulent Air Flow Downwind of a Model Forest Edge', *Boundary-Layer Meteorol.* **77**, 21–44.

Louka, P., Belcher, S. E., and Harrison, R. G.: 2000, 'Coupling between Air Flow in Streets and the Well Developed Boundary Layer Aloft', *Atmos. Environ.* **34**, 2613–2621.

Martilli, A., Clappier, A., and Rotach, M. W.: 2002, 'An Urban Surface Exchange Parameterisation for Mesoscale Models', *Boundary-Layer Meteorol.* **104**, 261–304.

Masson, V.: 2000, 'A Physically-Based Scheme for the Urban Energy Budget in Atmospheric Models', *Boundary-Layer Meteorol.* **94**, 357–397.

Meyers, T. and U, K. T. P.: 1986, 'Testing of a Higher-Order Closure Model for Modeling Airflow within and above Plant Canopies', *Boundary-Layer Meteorol.* **37**, 297–311.

Musson-Genon, L.: 1987, 'Numerical Simulation of a Fog Event with a One-Dimensional Boundary Layer Model', *Mon. Wea. Rev.* **115**, 592–605.

Ni, W.: 1997, 'A Coupled Transilience Model for Turbulent Air Flow within Plant Canopies and the Planetary Boundary Layer', *Agric. For. Meteorol.* **89**, 77–105.

Noilhan, J. and Planton, S.: 1989, 'A Simple Parameterization of the Land Surface Processes for Meteorological Models', *Mon. Wea. Rev.* **117**, 536–549.

Oikawa, S. and Meng, Y.: 1995, 'Turbulence Characteristics and Organised Motions in a Suburban Roughness Sublayer', *Boundary-Layer Meteorol.* **74**, 289–312.

Oke, T. R.: 1978, *Boundary Layer Climates*, Methuen and Co. Ltd., U.K., 435 pp.

Oke, T. R.: 1995, 'The Heat Island of the Urban Boundary Layer: Characteristics, Causes and Effects', in J. E. Cermak et al. (eds.), *Wind Climate in Cities*, Kluwer Academic Publishers, Dordrecht, pp. 81–107.

Raupach, M. R. and Shaw, R. H.: 1982, 'Averaging Procedures for Flow within Vegetation Canopies', *Boundary-Layer Meteorol.* **22**, 79–90.

Raupach, M. R., Antonia, R. A., and Rajagoplan, S.: 1991, 'Rough-Wall Turbulent Boundary Layers', *Appl. Mech. Rev.* **44**, 1–25.

Raupach, M. R., Coppin, P. A., and Legg, B. J.: 1986, 'Experiments on Scalar Dispersion within a Model Plant Canopy. Part I: The Turbulence Structure', *Boundary-Layer Meteorol.* **35**, 21–52.

Raupach, M. R., Finnigan, J. J., and Brunet, Y.: 1996, 'Coherent Eddies and Turbulence in Vegetation Canopies: the Mixing-Layer Analogy', *Boundary-Layer Meteorol.* **78**, 351–382.

Rotach, M. W.: 1993, 'Turbulence Close to a Rough Urban Surface. Part I: Reynolds Stress', *Boundary-Layer Meteorol.* **65**, 1–28.

Rotach, M. W.: 1995, 'Profiles of Turbulence in and above an Urban Street Canyon', *Atmos. Environ.* **29**, 1473–1486.

Roth M.: 2000, 'Review of Atmospheric Turbulence over Cities', *Quart. J. Roy. Meteorol. Soc.* **126**, 941–990.

Shafran, P. C., Seaman, N. L., and Gayno, G. A.: 2000, 'Evaluation of Numerical Predictions of Boundary Layer Structure during the Lake Michigan Ozone Study', *J. Appl. Meteorol.* **39**, 412–426.

Shaw, R. H. and Patton, E. G.: 2003, 'Canopy Element Influences on Resolved- and Subgrid-Scale Energy within a Large-Eddy Simulation', *Agric. For. Meteorol.* **115**, 5–17.

Shen, S. and Leclerc, M. Y.: 1997, 'Modelling the Turbulence Structure in the Canopy Layer', *Agric. For. Meteorol.* **87**, 3–25.

Taha, H.: 1999, 'Modifying a Mesoscale Model to Better Incorporate Urban Heat Storage: A Bulk Parameterization Approach', *J. Appl. Meteorol.* **38**, 466–473.

Therry, G. and Lacarrère, P.: 1983, 'Improving the Eddy Kinetic Energy Model for Planetary Boundary Layer Description', *Boundary-Layer Meteorol.* **25**, 63–88.

Wilson, J. D., Finnigan, J. J., and Raupach, M. R.: 1998, 'A First-Order Closure for Distributed Plant-Canopy Flows, and its Application to Winds in a Canopy on a Ridge', *Quart. J. Roy. Meteorol. Soc.* **124**, 705–732.

Zeng, P. and Takahashi, H.: 2000, 'A First-Order Closure Model for the Wind Flow within and above Vegetation Canopies', *Agric. For. Meteorol.* **103**, 301–313.